©2017

Zhaocheng Lu

PROJECTION MICRO-STEREOLITHOGRAPHY OF TEMPERATURE

RESPONSIVE PNIPAAM HYDROGEL

By

ZHAOCHENG LU

A thesis submitted to the

Graduate School-New Brunswick

Rutgers, The State University of New Jersey

In partial fulfillment of the requirements

For the degree of

Master of Science

Graduate Program in Mechanical and Aerospace Engineering

Written under the direction of

Howon Lee

And approved by

_____

_____

_____

New Brunswick, New Jersey

January 2017

ABSTRACT OF THE THESIS

Projection Micro-stereolithography of Temperature Responsive PNIPAAm Hydrogel

by Zhaocheng Lu

Thesis Director:

Howon Lee

Poly(N-isopropylacrylamide) (PNIPAAm) is one of the most popular temperature responsive hydrogel which is widely used in many research fields. However, the application of PNIPAAm is significantly limited because of lack of suitable three-dimensional (3D) fabrication method.

Projection Micro-StereoLithography (PµSL) is an additive manufacturing method for fabricating 3D complex micro structures. Various photo-curable resins have been processed and fabricated into 3D micro structures by PµSL.

This thesis applies PµSL technique to the PNIPAAm temperature responsive hydrogel. This method can not only realize the complex three-dimensional PNIPAAm microstructures but also help reduce responsive time of PNIPAAm structures by allowing for micro scale manufacturing.

Firstly, the fundamental principle of PNIPAAm temperature responsive property is investigated by temperature dependent swelling behavior experiments.

Then the effects of various PµSL process parameters on temperature dependent swelling behavior are investigated to realize the control of temperature responsive property of 3D PNIPAAm structures fabricated by PµSL. Several 3D printed PNIPAAm structures are also shown.

Finally, it is demonstrated that PNIPAAm-alginate double-network hydrogel enhances the mechanical property while maintaining the temperature responsive property. Sequential cross-linking method is proposed to fabricate 3D double-network hydrogel using PµSL.

ACKNOWLEDGEMENTS

First of all, I would like to thank my advisor, Prof. Howon Lee, for his continuous support and professional guidance during my Master degree research project and my life in United State.

My deep appreciation extends to the rest of my thesis committee, Prof. Aaron Mazzeo and Prof. Jonathan Singer for their willingness to join my thesis committee and the time that they took out of their schedules to review my thesis.

A lot of thanks also goes to my colleagues in Prof. Lee's group. Daehoon Han and I have worked together on the same project and I have learned a lot of knowledge from him. Chen Yang always provide me some useful suggestion in experiment design and results analysis. Manish, Ridhish and Ishan are also great to work with and have helped me at various points throughout my research.

Mengqi Wang provides continuous encouragement throughout my years of study and for her support, I am especially grateful.

Most importantly, my family's support throughout my whole life led me to this point. This accomplishment would not be possible without their kind friendship and guidance.

TABLE OF CONTENTS

LIST OF TABLES

LIST OF ILLUSTRATIONS

1. Introduction

1.1 Stimuli responsive hydrogels

1.1.1 Hydrogel

Hydrogels are three-dimensional network of polymer chains with the ability of absorbing a large amount of solvent while maintaining their dimensional stability without dissolution. The capability of absorbing the solvent to their networks arises from the hydrophilic functional group attached to their polymeric backbone. The cross-links between the network chains result in the resistance to dissolution in their swollen state [1]. In the presence of cross-linking points, solubility of the hydrophilic linear polymer chains is counter-balanced by the retractive force of elasticity induced by cross-linking points of the network. Swelling reaches at an equilibrium point as these forces becomes equal [2]. Further, hydrogels are capable of swelling or de-swelling reversibly in solvent.
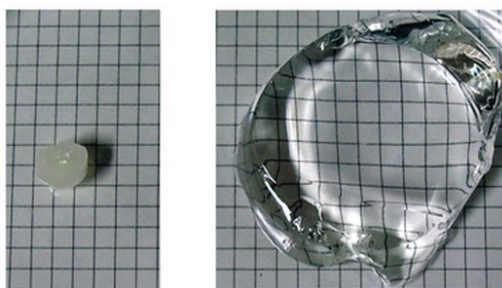
Figure 1-1 Dry gels (left) and wet gels (right) swollen in solvent [3]

Hydrogels have received a considerable attention due to the reliability in a wide range of applications. Hydrogel can create a hydrated environment. Hydrogel has a lower interfacial tension and tissue-like physical properties [4]. The tunable property of hydrogel is similar to the native extracellular matrix [5]. Hydrogel can entrap and release molecules in a controlled manner [6].

1.1.2 Stimuli responsive hydrogel

Some hydrogels are found with the controllable swelling or de-swelling in response to a variety of changes in external environmental conditions.

Stimuli responsive hydrogels are defined as the hydrogels that undergo relatively large and abrupt change reversibly in their swelling behavior, network structure, permeability and/or mechanical strength in response to small environmental changes [7].

A variety of stimuli, either physical types or chemical types, can result in hydrogel properties change. Therefore, stimuli responsive hydrogels can be further classified as figure 1.2 shows.

```
┌──────────┐ ┌──────────┐      ┌──────────┐ ┌──────────┐ ┌──────────┐
│   pH     │ │ Glucose  │      │ Antigen  │ │  Enzyme  │ │  Ligand  │
│responsive│ │responsive│      │responsive│ │responsive│ │responsive│
│hydrogels │ │hydrogels │      │hydrogels │ │hydrogels │ │hydrogels │
└──────────┘ └──────────┘      └──────────┘ └──────────┘ └──────────┘

      ┌────────────┐                  ┌────────────┐
      │  Chemical  │                  │Biochemical │
      │ responsive │                  │ responsive │
      │            │                  │            │
      │  hydrogels │                  │  hydrogels │
      └────────────┘                  └────────────┘

                    ┌──────────┐
                    │  Smart   │
                    │Hydrogels │
                    └──────────┘
                    ┌──────────┐
                    │ Physical │
                    │responsive│
                    │hydrogels │
                    └──────────┘

┌─────────┐┌─────────┐┌─────────┐┌─────────┐┌─────────┐┌─────────┐
│Pressure ││Tempera- ││Ultrasound││Magnetic ││ Electric ││Light (UV,│
│responsive││ ture    ││responsive││  field  ││  field   ││   IR)    │
│hydrogels ││responsive││hydrogels ││responsive││responsive││responsive│
│          ││hydrogels ││          ││hydrogels ││hydrogels ││hydrogels │
└─────────┘└─────────┘└─────────┘└─────────┘└─────────┘└─────────┘
```

Figure 1-2 Classifications of stimuli responsive hydrogel [7].

The chemical stimuli, such as pH, ionic factors and chemical agents, will change the interactions between polymer chains or between polymer chains and solvent at the molecular level. The physical stimuli, such as temperature, electric or magnetic fields, and mechanical stress, will affect the level of various energy sources and alter molecular interactions at critical onset points [7].

1.1.3 Temperature responsive hydrogel

In this thesis, we are mainly interested in the temperature responsive hydrogels.

Temperature responsive hydrogels can be classified as positive or negative temperature responsive systems. Positive temperature responsive hydrogels show phase transition at critical temperature called the upper critical solution temperature (UCST). Hydrogels made from polymers with UCST shrink when cooled below their UCST. An example of USCT, such as PLA-PEG-Biotin, was applied for the fabrication of cell carriers [8]. Negative temperature responsive hydrogels have a lower critical solution temperature (LCST). These hydrogels shrink upon heating above their LCST. For example, chemically cross-linked hydrogels based on methylcellulose (MC), HPMC, hydroxypropylcellulose, and carboxymethylcellulose are often used for drug release applications [9].

Generally, LCST is addressed in terms of phase transition temperature, namely the temperature at which the polymer suddenly shrinks. This property has made temperature responsive polymers useful for many applications, such as controlling bacterial aggregation [10] and protein adsorption and release [11].

If the LCST of the polymer is tunable within a wide temperature range, it can be more useful for a variety of applications. One approach often used to control the LCST of a polymer is to make a co-polymer by adding a second monomer with different hydrophilicity. This will lead to a co-polymer with variable LCST depending on the compositions of different components [12].

1.1.4 PNIPAAm hydrogel

Poly(N-isopropylacrylamide) (PNIPAAm) is the most widely used and extensively studied negative temperature responsive hydrogel. PNIPAAm hydrogel has both hydrophobic and hydrophilic groups in its network structure. As Fig. 1.3 shows, when temperature is below the LCST (around 32~35 °C), hydrophilic groups on PNIPAAm chains form hydrogel bond with water molecules. Therefore, the PNIPAAm chains extend and network structure swells. When temperature is above the LCST, the hydrated and extended PNIPAAm chains collapse into a hydrophobic state with simultaneous release of the bound water molecules. Therefore, the network structure shrinks.
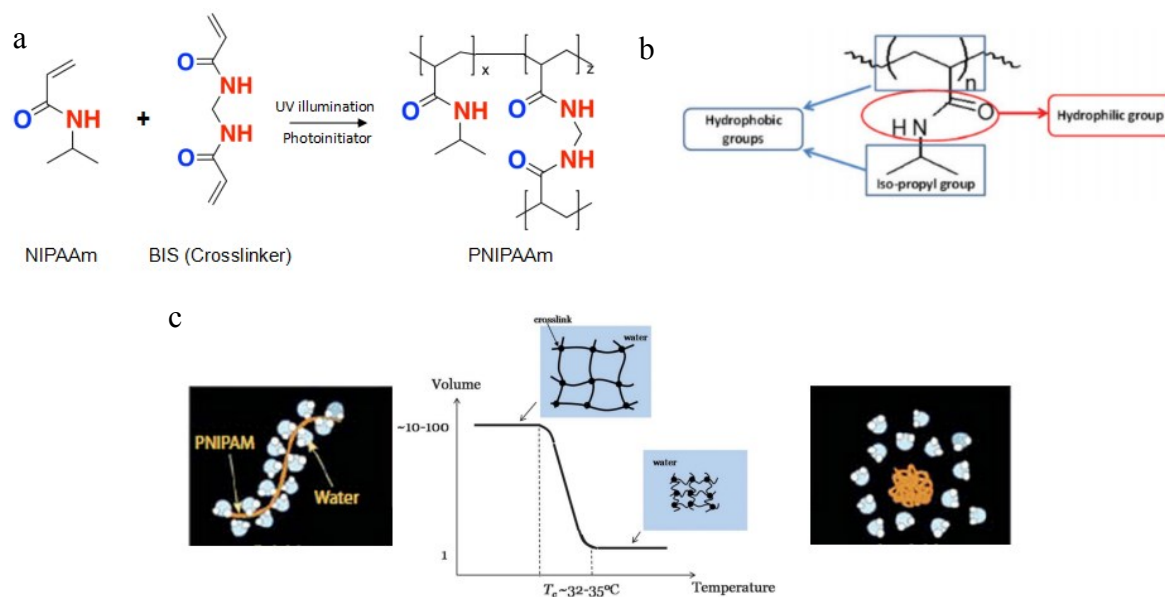
Figure 1-3 Cross-linked hydrogel polymerization of PNIPAAm (a), chemical structure of PNIPAAm (b) and Temperature-responsive mechanism of PNIPAAm (c) [13] [14]

Currently, PNIPAAm and PNIPAAm based co-polymers are extensively studied and used in a variety of applications:

Microfluidic valve. PNIPAAm hydrogel has been used to create a self-actuated thermo-responsive hydrogel valve. When the temperature of PNIPAAm gel is increased above the critical temperature, the hydrogel is in the de-swelled state and the conduit is open to let liquid flow. When the temperature decreased below the critical temperature in the presence of aqueous solution, the hydrogel swelled and the conduit was blocked [15] (Fig. 1.4 I). Anisotropic shrinkage PEG–PNIPA hydrogel is used as a valve in a fluid regulation device without being washed away with fluid [16] (Fig. 1.4 II).

Temperature-triggered Actuators. Bilayer nanofiber mat made by thermoresponsive polymer pNIPAM-4-acryloylbenzophenone (P(NIPAM-ABP)) and non-responsive polymers Thermoplastic polyurethane TPU can work as superfast actuator with large scale movements [17] (Fig. 1.4 III). Bilayer structure made by temperature responsive copolymer poly(N-isopropylacryla-mide-co-acrylic acid) (P(NIPAM-AA) and the passive layer poly-(methylmethycrylate) (PMMA) is used for highly complex, self-folding 3D objects. The folding motion is realized by proper design of the bilayer's external shape [18] (Fig. 1.4 IV).

Micro-lenses. PNIPAAm hydrogel is integrated into a microfluidic channel of liquid lens system and serves as the container for a water droplet. The water–oil interface forms the liquid microlens. The expansion and contraction of the hydrogel regulates the shape of the water microlens. The microlens is divergent between 23 °C and 33 °C. However, between 33 °C and 47 °C, the microlens becomes convergent [19] (Fig. 1.4 V), demonstrating tunable focal length.

Drug delivery agent. Poly(N-isopropylacrylamide-co-butylmethacrylate-co-acrylic acid) (P(NIPAM-co-BMA-co-AAc)) have been used for intestinal delivery of calcitonin. The peptide or hormone is immobilized in polymeric beads and remains stable while passing through the stomach. Then in the alkaline intestine the beads disintegrate and the drug is released [20].

Biosensor. Poly(N-isopropylacrylamide-co-4′-acrylamidobenzo-18-crown-6) (P(NIPAM-AABC)) microgels are synthesized as lead sensor using the phenomenon that the existence of cations increases the swelling degree of the microgels. The microgels show a good sensitivity to lead by swelling to 430% of its original volume in the presence of Pb^{2+} [21].

Microgel film for cell collection and release. Mammalian cells can be easily cultured on PNIPAAm at 37°C because of phase change of PNIPAAm. When the temperature is lower than PNIPAAm's lower critical solution temperature, cells detach in intact cell sheets. This detachment method is better than traditional enzymatic digestion and mechanical scraping [22]. Thermosensitive PNIPAAm microgel films are able to provide switchable cell adhesion for convenient harvesting of cultivated cells. The microgels favor cell adhesion and proliferation when temperature is slightly above the LCST. Switching back to room temperate results in repulsive forces and allows removal of the cells from the substrate by gentle rinsing [23] (Fig. 1.4 VI).

I

Top view | Side view

(a) ON, T > T_c

(b) OFF, T < T_c

gel

Microfluidic valve

II

as spun | water, 40°C | water, 4°C

TPU40-NIPAM15
TPU40-NIPAM30
TPU40-NIPAM70
TPU40-NIPAM100

Temperature-Triggered Actuators

III
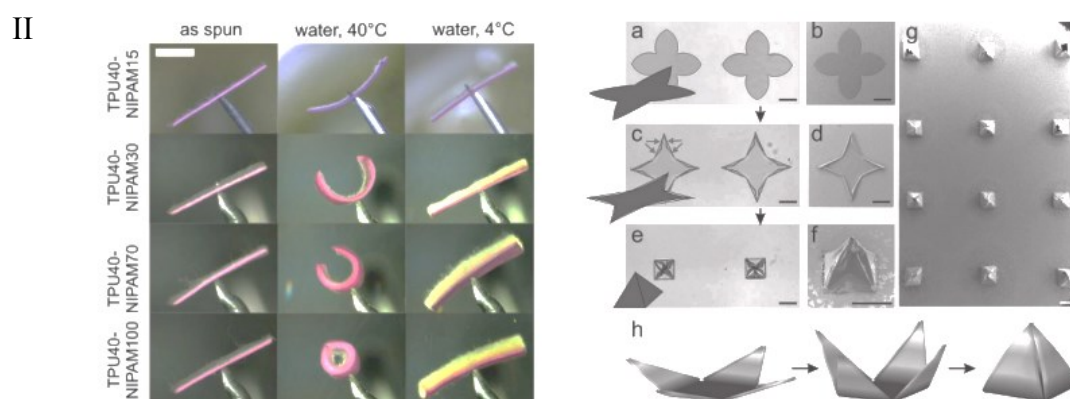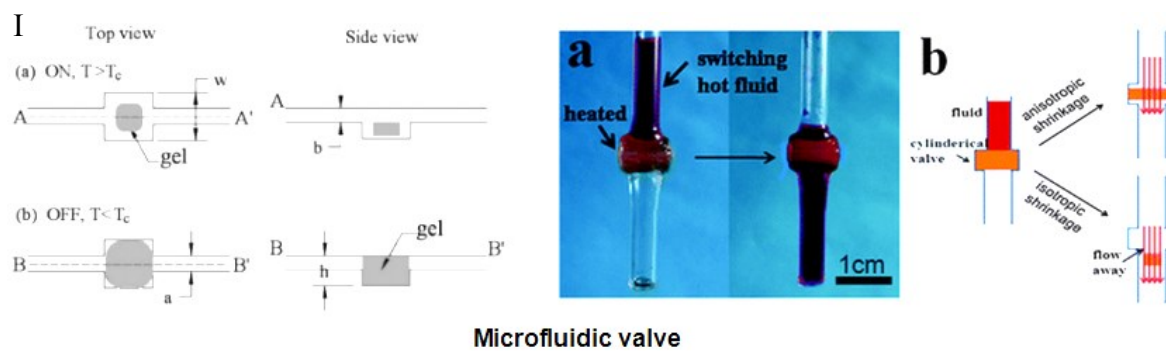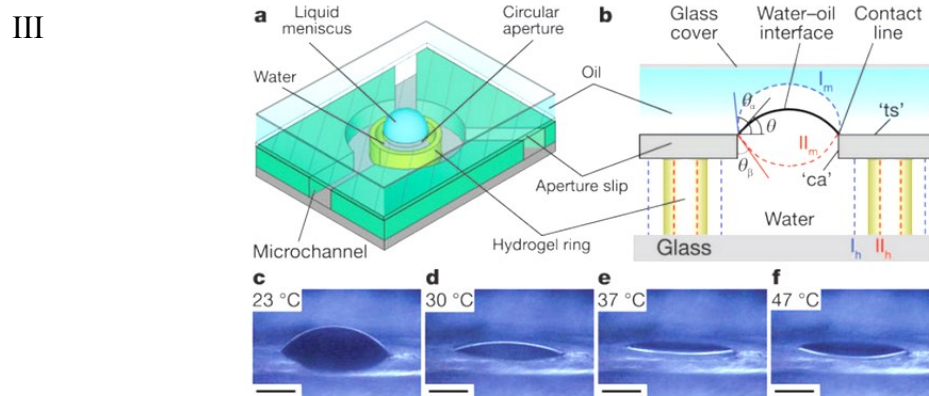
Micro-lenses

IV
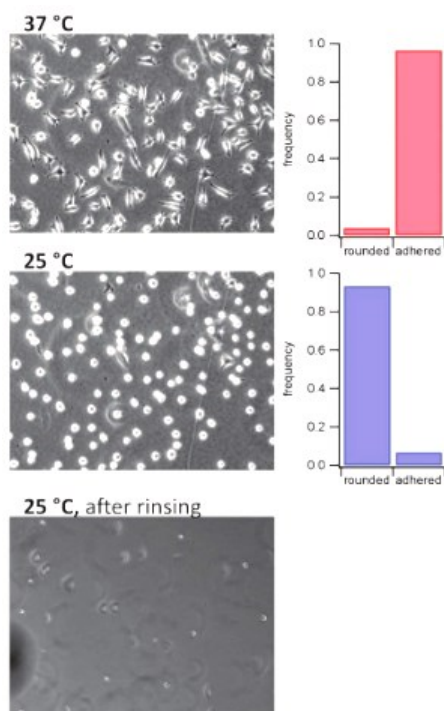
Film for cell adhesion and release

Figure 1-4 PNIPAAm application. Microfluidic valve [15] [16]. Temperature-triggered Actuators [17] [18]. Micro-lenses [19]. Microgel film for cell collection and release [23]

1.1.5 PNIPAAm fabrication methods

PNIPAAm hydrogels have the widespread applications in different engineering areas not only due to the temperature responsive property but also their easy fabrication methods. PNIPAAm hydrogels are able to be synthesized via free radical polymerization. Thermal-polymerization is one type of free radical polymerization method. Typically, during the polymerization, thermal initiator is used under moderate heating at certain temperature for effective generation of free radicals. For example, the polymerization of NIPAAm monomer and N,N'-methylenebis(acrylamide) (BIS) cross-linker is initiated by a water soluble, free-radical initiator such as ammonium persulfate (APS) or 2,2′-azobis(amidinopropane) dihydrochloride (V50) at 60 to 70 °C [24].

Photo-polymerization is another type of free radical polymerization method. As Fig. 1.5 shows, during the initiation process, the photo-initiator absorb incident photons and generate free radicals under UV illumination. During the propagation process, the free radicals

combine with the monomer molecules to form the reactive molecules. These reactive

molecules continue to react with adjacent monomer molecules to form longer polymeric

molecules. Finally, the polymeric molecules keep growing until two of them combine and

terminate the reaction.
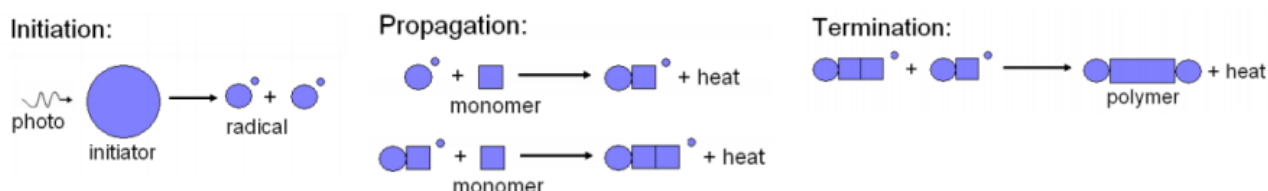
Figure 1-5 Photo-polymerization process

We use photo-polymerization method to fabricate PNIPAAm samples in this thesis. NIPAAm

UV curable resin mainly consists of monomer, cross-linker and photo-initiator. Because the

cross-linker also has carbon-carbon double bond vinyl group which radical initiation works

best on, it can also participate in polymerization process and finally results in the network

PNIPAAm polymer structure.

However, PNIPAAm fabrication is limited to two-dimensional structure by using traditional

fabrication method, such as molding. Cuboid, cylinder or simple stacks of certain shape are

often seen in the PNIPAAm structures.

Recently, some groups have tried to fabricate three-dimensional structures using origami

approach. For this method, tri-layer two-dimension structure is fabricated first. PNIPAAm is

sandwiched between two rigid patterned non-thermal responsive gels. PNIPAAm works as

the actuator for folding motion based on its temperature-dependent swelling property. The

two patterned non-thermal responsive layers decide the property of folding motion, such as

location and angle. Therefore, the reversible three-dimensional structure is realized by

temperature change [25] [26] (Fig. 1.4 I and II).

Other groups printed programmable bilayer architectures consisting of multiple fibrils lines

with anisotropic swelling property. PNIPAAm composite ink containing cellulose fibrils is

the printing material. During printing, these fibrils undergo shear-induced alignment as the

ink flows through the deposition nozzle, which leads to printed material with anisotropic swelling behavior. The anisotropic swelling and the design of geometry induces the complex three-dimensional structure [27] (Fig. 1.4 III).
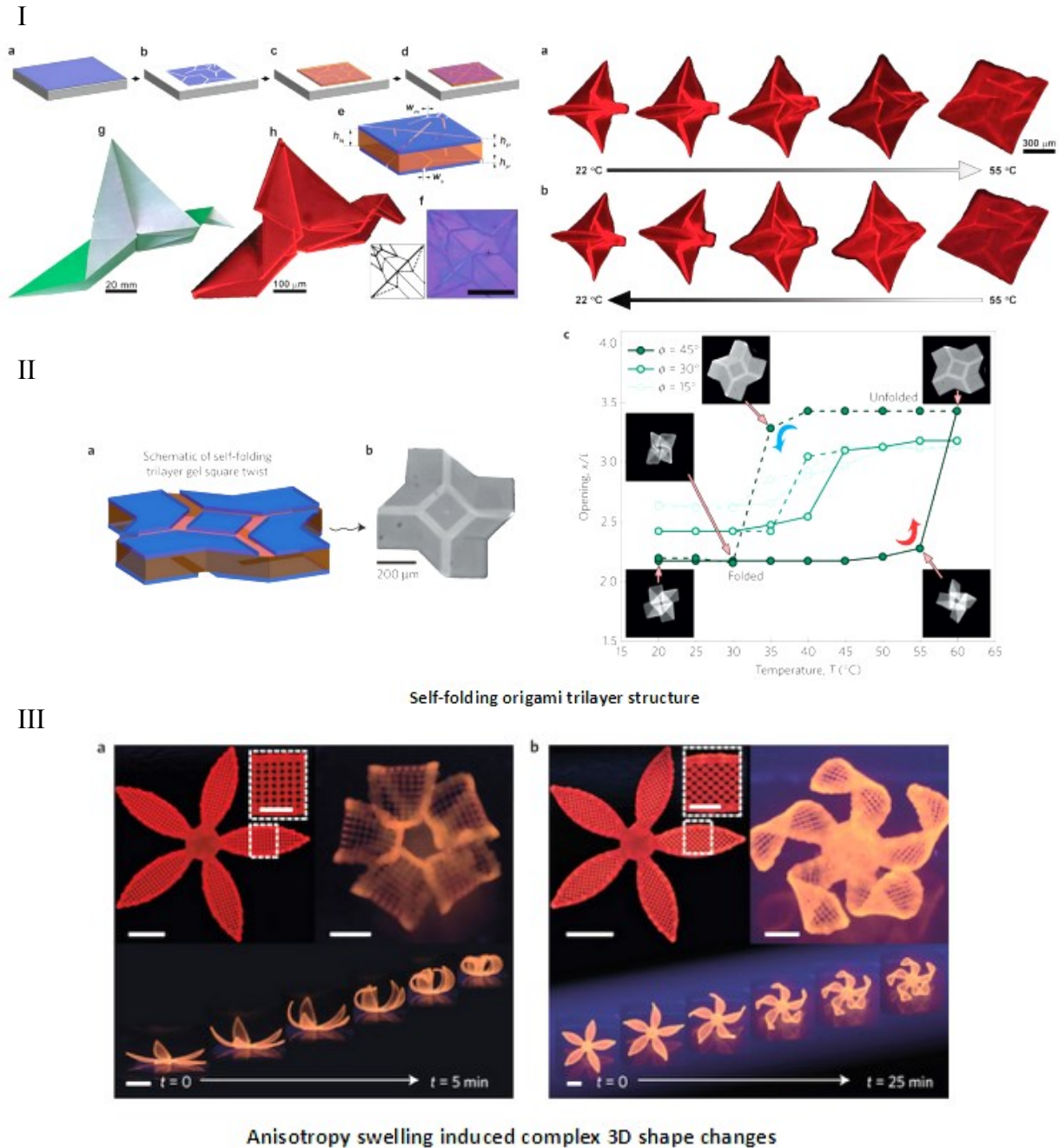
Figure 1-6 Fabrication methods of PNIPAAm 3D structure. Self-folding origami tri-layer structure [25] [26]. Anisotropy swelling induced complex 3D shape changes [26]

Nevertheless, for the above mentioned methods, PNIPAAm material itself is in still simple two-dimensional structure and complex simulation models are needed to precisely predict how the structures will swell and transform.

Currently, there is an increasing need for 3D micro-fabrication method for PNIPAAm. For example, in tissue engineering, the complicated biomimetic micro structures are needed. A combination of hydrogel and 3D printing can make more biocompatible and benign niche for cells culture in vitro [28].

1.2 Projection micro- stereolithography (PµSL) technique

In this thesis, we want to apply additive manufacturing method in temperature responsive hydrogel 3D structure fabrication.

1.2.1 Additive manufacturing

3D printers have been developed in many different printable sizes and printable materials. On the one hand, news reported that a Chinese company printed a full-sized house measuring 200 square meters within a few hours [29]. On the other hand, *Nanoscribe* produced a new generation of laser lithography systems which are able to print arbitrarily complex shaped structures with finest feature sizes in the sub-micrometer range [30].
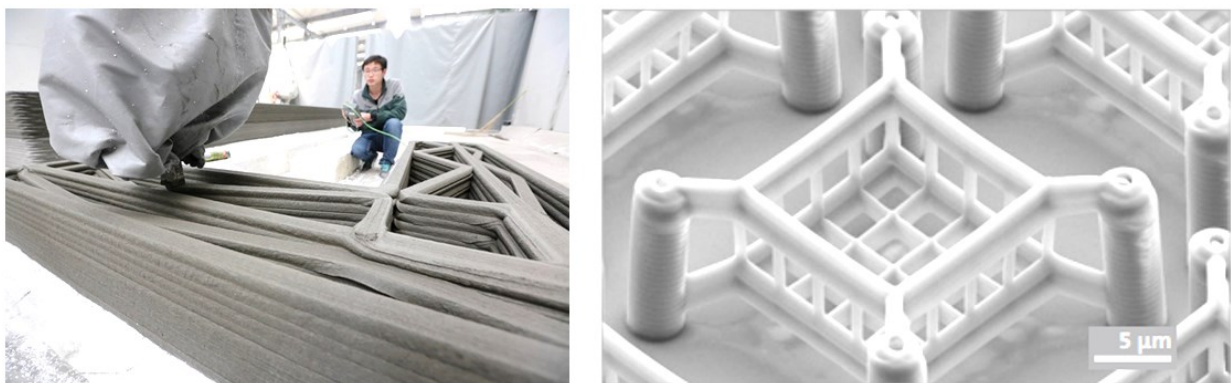
Figure 1-7 3D printer used for the construction measures 6.6 m x 10 m and is 150 m long and printing process (left) [29]. Biocompatible cell scaffold and C 180 fullerene-like polymer microstructure (right) [30]

In between the large end and small end of the sizes, a variety of printing methods are available for many different kinds of materials.

Fuse deposition modeling (FDM) technique uses a small temperature-controlled extruder to force out a thermoplastic filament material and deposit the semi-molten polymer onto a platform in a layer by layer process [31]. Most commonly used materials in FDM is ABS and Poly-Carbonate (PC). Metallic and ceramic materials have also been used by mixing the metallic and ceramic powders with organic binder system. Further processing to remove the organic parts are needed [32].

Selective laser sintering (SLS) technique uses a laser as the power source to sinter powdered material. The laser beam is selectively scanned over the powder surface following the cross-sectional profiles, binding the material together to create a solid structure. Subsequent layers are built directly on top of previously sintered layers with new layers of powder being deposited via a roller on top of the previously sintered layer [33]. SLS can print parts from a relatively wide range of powder materials including polymers and metals such as nylon [34] and metal [35].
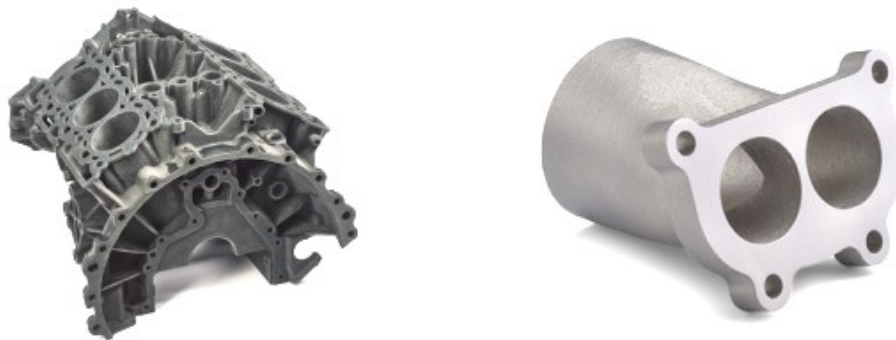
Figure 1-8 3-D printed components by FDM (lift, ABS) and SLS (right, metal) (credit to Stratasys company)

In this thesis, we pay more concentration on high resolution, three-dimensional, polymeric material fabrication methods.

To achieve the capability of high resolution three-dimensional fabrication, some manufacturing techniques have been reported. Three-dimensional laser chemical vapor deposition (3D-LCVD) [36] and electrochemical fabrication (EFAB) [37] realize the complex three-dimensional microstructure fabrication. However, these two techniques suffer from the limited materials that can be incorporated with these processes. Photo-curable polymers cannot be 3D printed in these methods.

Micro-stereolithography (μSL) [38] is able to fabricate high precision microstructure. 3D model designed with CAD software is sliced into a series of 2D layers. The numerical control (NC) code generated from each 2D file is then executed to control a motorized x-y stage carrying UV curable solution. The focused scanning UV beam is absorbed by curable solution leading to the polymerization. However, the x–y scanning process significantly increases the processing time and cost.

Recently, syringe-based printing system (syringe tip size is 0.337 mm in diameter) coupled with UV-curing system successfully printed a three-dimensional temperature-responsive valve with ability of flow rate control as Fig. 1.9 shows [39]. However, the fixed syringe tip size strictly restricted the resolution of printed structure. The low resolution of commercial printers makes it difficult to build small-size structure which has relatively short diffusion length to minimize the actuation time. In addition, the long diffusion length of the structure may induce the trapping of the water molecules when it shrinks. The different shrinkage condition between outer and inner section of structure may lead to unwanted structural deformation or blisters.

Figure 1-9 Printing process of the valve (left). The valve swollen in water at 20 °C (middle) and swollen in water at 60 °C (right) [39]

1.2.2 PµSL and application

Projection micro-stereolithography (PµSL) employs the digital mask to generate patterns of light, which is different from traditional stereolithography method. This change not only eliminates the time and cost needed to spend on intensive steps in traditional lithography such as mask production, replacement and alignment, but also enhances capability of manufacturing complex three-dimensional structures at micron scale.

Generally speaking, PµSL system consists of four major components: optic part (UV light source, digital mask, a set of lenses and CCD camera), chamber part (sealed chamber containing resin and resin supply control), motion part (motorized translation stage) and control part (computer with LabVIEW codes).

Mask patterns are dynamically generated on chip based on the sliced BMP images of printed structure. The light illuminated on the chip is patterned according to the dynamic mask. Then, the patterned light is transferred through a reduction lens. Finally, a projection image with a reduced feature size is formed on curable resin surface. The illuminated area is polymerized simultaneously under one exposure. After the fabrication of one layer, the sample plate is immersed into the photo-curable resin and the new layer is fabricated on top of the existing structure [40].

PµSL technique is compatible with various photo-curable materials. Many fascinating works and projects have been done by PµSL technique.

Xia et al. printed solvent-driven poly(ethylene glycol) diacrylate (PEGDA) polymeric micro beam device with capillary network. Compared with traditional silicon MEMS devices, this device can achieve much higher displacement with respect to the length of the beam without sacrificing the actuation speed [41] (Fig. 1.4 I).

Lee et al. printed poly(ethylene glycol) diacrylate (PEGDA) hydrogel microtubes. By modifying the dimensional parameters of the microtube, the swelling-induced circumferential buckling pattern can be well controlled [42] (Fig. 1.4 II).

Zheng et al. printed 1,6-hexanediol diacrylate (HDDA) or poly(ethylene glycol) diacrylate (PEGDA) polymer microlattice template first. Then convert the structure to metallic

microlattice by metal coating on as formed photopolymer. The polymer template is removed by thermal decomposition [43] (Fig. 1.4 III).

Ge et al. printed methacrylate (MA) based shape memory polymer architectures. The printed 3D structures exhibit well-controlled shape memory behavior over time in responsive to thermal stimulus. This PµSL printing with active material is also referred to as 4D printing [44] (Fig. 1.4 IV).

I
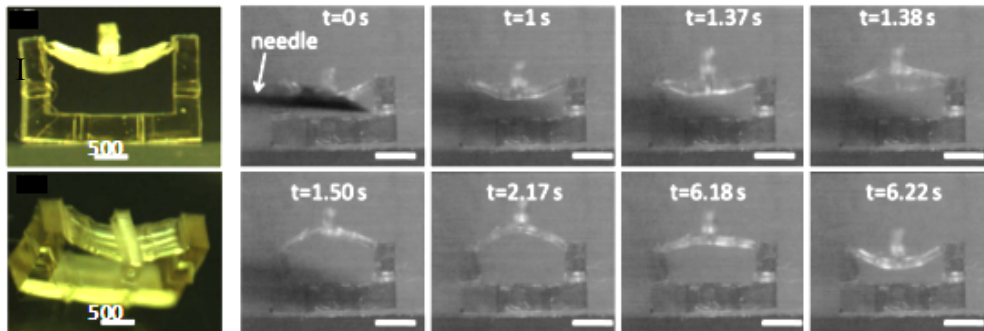
PuSL printed PEG bistable beam device (left). time frames of the bistable beam device actuated by a drop of aceton. (right)

II
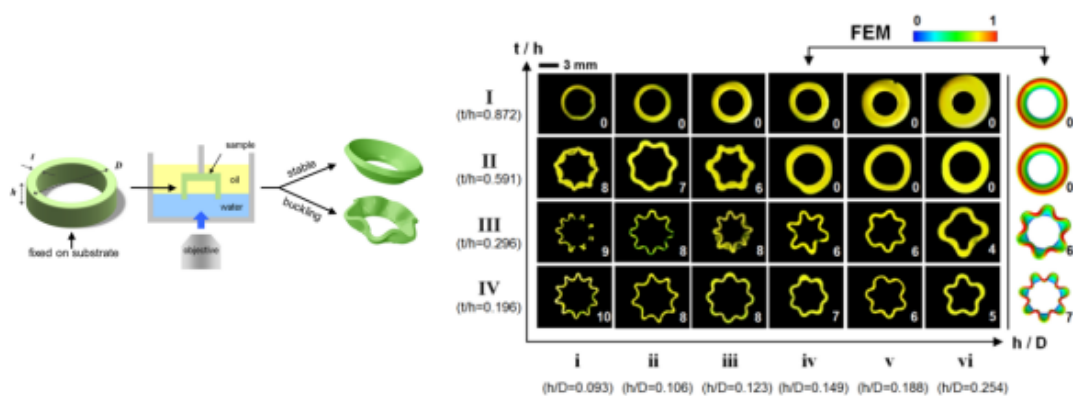
Characteristic dimensions of PuSL printed tubular gel and experimental setup (left). Patterns formed in swelling experiment (right).

III
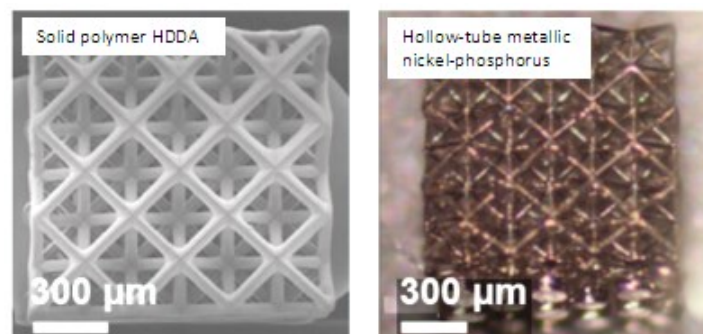
Metallic lattices were generated by electroless nickel plating on the PµSL printed HDDA.

IV
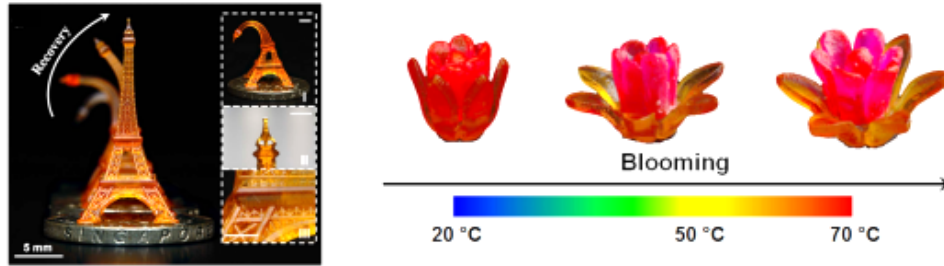
PuSL printed SM Eiffl tower and recovery (left). Sequential shape recovery by printing a multimaterial flower whose inner and outer petals have diffrent T_g s

Figure 1-10 PuSL system application (From top to bottom [41] [42] [43] [44])

1.3 Outline of the thesis

The objective of this thesis is to apply Projection Micro-StereoLithography (PμSL) method in PNIPAAm 3D micro structure fabrication.

In Chapter 2, to better understand the material, we investigate the fundamental principle of temperature responsive property of PNIPAAm hydrogel. We propose principles of the swelling at low temperature and shrinkage at high temperature and design two sets of experiments to prove them. Besides, chemicals in photo-curable NIPAAm resin are introduced. The fabrication method of fully cured PNIPAAm samples and the measurement method of PNIPAAm sample size at different temperature are presented.

In Chapter 3, we introduce the study on the temperature responsive property of 3D printed PNIPAAm. The effects of all the process parameters in the PμSL printing method, such as chemicals and printing process parameters, on temperature responsive property are investigated to realize the control of swelling behavior of printed PNIPAAm samples. Meanwhile, PμSL printing system and its printing process are presented. Demonstration examples are introduced to show the applications of PμSL printed PNIPAAm structures.

In Chapter 4, we introduce the method of forming double-network structure to improve the mechanical property of PNIPAAm hydrogel. The feasibility of this method is investigated by fabricating PNIPAAm-alginate double-network hydrogel. By performing tensile tests, we can find the mechanical property information. The swelling ratio test is also performed to investigate whether the temperature responsive property is maintained. Then we propose sequential cross-linking method to realize the 3D printing of double-network hydrogel with

improved mechanical property. The mechanical property and temperature responsive property of sequentially cross-linked PNIPAAm-alginate double-network hydrogel are measured to prove the feasibility of this method.

In Chapter 5, we make a conclusion of all the studies in this thesis and present some future works.

2. Temperature responsive swelling of PNIPAAm

In order to make use of PNIPAAm hydrogel, we have to fully understand the fundamental principle of temperature responsive behavior first.

In this chapter, we investigate the effects of different chemicals in photo curable resin on the temperature dependent swelling behavior.

We hypothesize that the molar ratio of NIPAAm monomer to cross-linker the photo-curable resin determines the swelling at low temperature and the concentration of chemical species in a solvent determines the shrinkage at high temperature. We design two sets of experiments to prove these hypotheses. Molar ratio and concentration of chemicals in photo-curable NIPAAm resin are carefully designed. PNIPAAm samples are fabricated by UV oven using these NIPAAm resins. The temperature dependent swelling ratios are measured by our custom-built measurement system.

2.1 Temperature dependent swelling behavior

Firstly, we hypothesize that the swelling of polymer network at low temperature is determined by the length of a polymer chain between cross-linking sites and this length is further determined by the molar ratio of monomer to cross-linker.

For freely jointed chain polymer model, a polymer chain is a series of N straight segments of a given length l as depicted in Fig. 2.1. The segment length can be fixed at constant value and assumed to be equal in every segment for simplicity [45]. The end-to-end distance of polymer chain, R, represents the size of the polymer chain. For freely jointed chain model, the end-to-end distance of polymer chain can be expressed by the following equation:

$$R = l \cdot \sqrt{N}$$
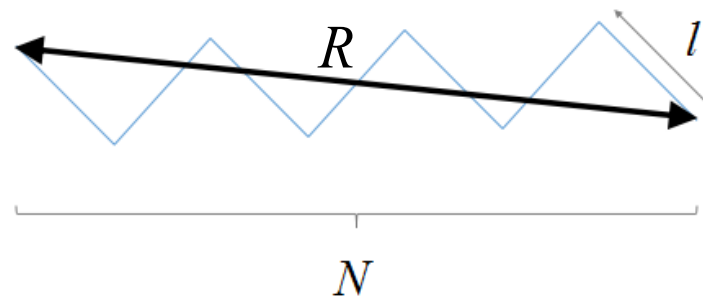
Figure 2-1 Schematic of polymer chain as freely jointed chain model.

For network polymer, as Fig. 2.2 left shows, cross-linkers bind PNIPAAm chains together to form a network structure. The molar ratio of NIPAAm monomer to cross-linker determines the length of a polymer chain bound between two cross-linking sites. The length of this polymer chain mainly determines the stretchability of the network structure and therefore determines the swelling size of polymer at low temperature.

For example, when we increase cross-linker concentration in the resin, more cross-linkers will be able to participate the cross-linking process, resulting in decreased length of polymer chain between cross-linking sites because the number of segments in polymer chains, N, decreases. The shorter chain usually has lower stretchability of the polymer network structure resulting in less room to accommodate water at low temperature.

Secondly, we hypothesize that the shrinkage of polymer network at high temperature is determined by the concentration of chemical species in solvent. Because the concentration of NIPAAm monomer is much higher than that of any other chemical species in solvent, we hypothesize that the shrinkage of polymer network at high temperature is mainly determined by the NIPAAm concentration in solvent.

At high temperature, as Fig. 2.2 shows, water molecules are expelled out of the network, leaving a crumpled polymer network. The volume of shrunken polymer network after losing significant portion of water at high temperature is therefore determined by the volume of chemical species in the solvent. The volume of chemical species in the solvent is determined by the chemical species concentration in the solvent and primarily determined by the NIPAAm concentration in the solvent.
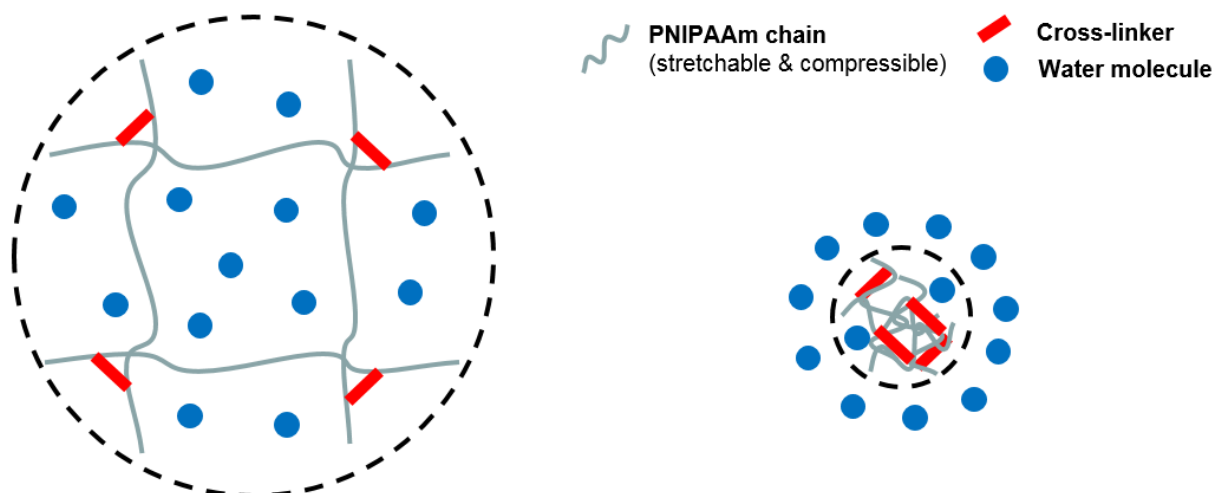
Figure 2-2 Swollen network at low temperature (left). Shrunken network at high temperature (right).

Therefore, we may independently control the swelling behavior of PNIPAAm at low temperature by controlling the molar ratio of NIPAAm monomer to cross-linker and the shrinkage behavior of PNIPAAm at high temperature by controlling the concentration of chemical species in the solvent.

We can change the molar ratio of NIPAAm monomer to cross-linker to realize the independent control of swelling at a low temperature. By increasing cross-linker concentration and keeping NIPAAm monomer (the main component in resin) concentration constant, the swelling size at low temperature will decrease but the shrinkage size at a high temperature will remain almost constant as Fig. 2.3 shows.

Similarly, we can change the concentration of chemical species in the solvent to realize the independent control of swelling at low temperature. By increasing chemical species concentration and keeping the molar ratio of NIPAAm monomer to cross-linker constant, the swelling size at low temperature will be kept almost constant but the shrinkage size at high temperature will increase as Fig. 2.4 shows.
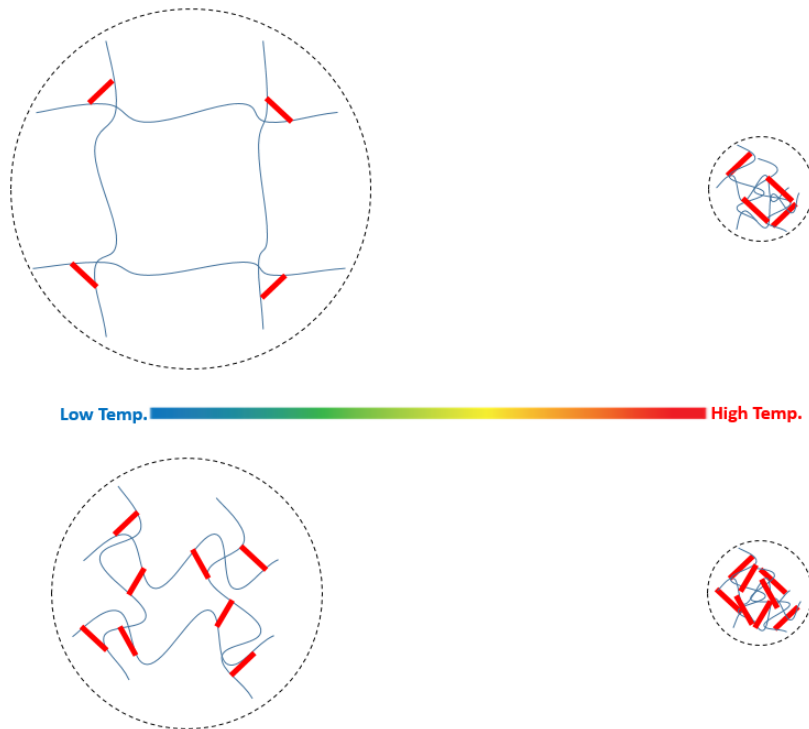
Figure 2-3 Effect of the ratio of monomer to cross-linker on the polymer network structure. Red bars indicate cross-linker whose length are unchangeable. Blue curly lines are polymer molecular chains which are stretchable and compressible
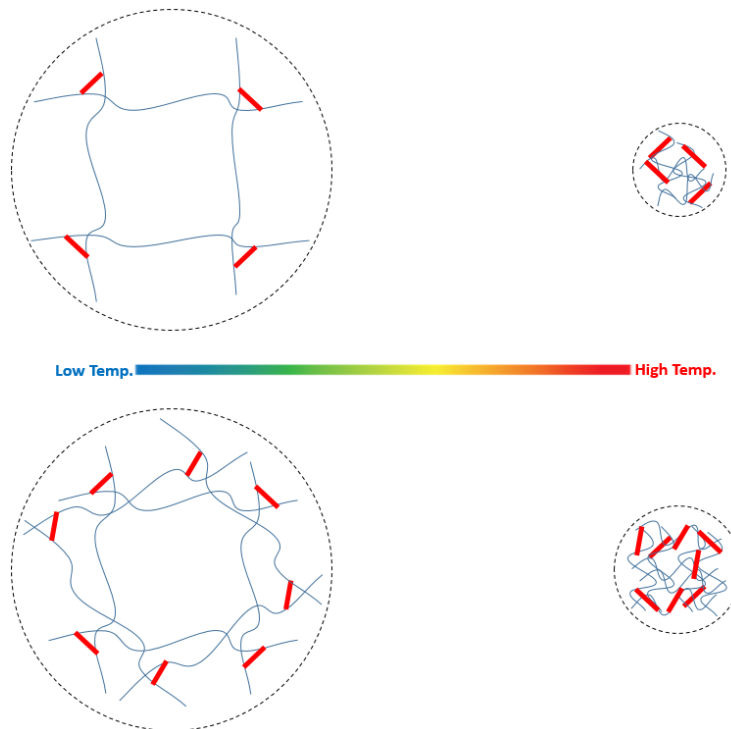
Figure 2-4 Effect of density of monomer in photo-curable resin on the polymer network structure. Red bars indicate cross-linker whose length are unchangeable. Blue curly lines are polymer molecular chains which are stretchable and compressible

2.2 Materials and Methods

To study temperature dependent swelling behavior of PNIPAAm hydrogel, we prepared photo-curable NIPAAm resin.

Photo-curable NIPAAm resin is composed of NIPAAm monomer, cross-linker, photo initiator, photo absorber and solvent. To investigate the principle of temperature dependent swelling behavior, fully cross-linked PNIPAAm samples are fabricated by a UV oven.

2.2.1 Materials

N-isopropylacrylamide (NIPAAm) (*Fisher Scientific*), N,N'-Methylene-bis(acrylamide) (*Sigma-Aldrich*), Phenylbis (2,4,6-tri-methylbenzoyl) phosphine oxide (*Sigma-Aldrich*) and Sudan I (*Sigma-Aldrich*) are dissolved in ethanol (*Sigma-Aldrich*) to form photo-curable NIPAAm resin.
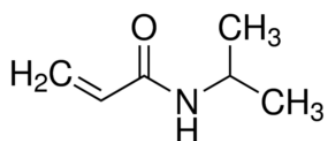
N-isopropylacrylamide (NIPAAm)
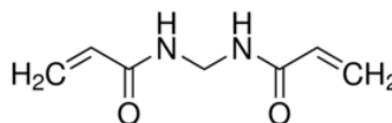
N,N'-Methylene-bis(acrylamide)
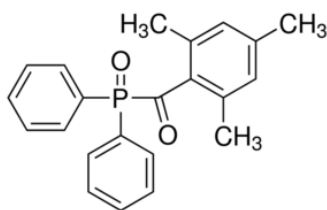
Phenylbis (2,4,6-tri-methylbenzoyl) phosphine oxide
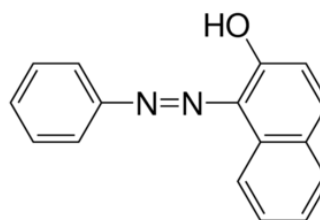
Sudan I
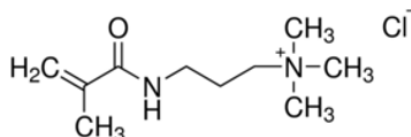
Methacrylamidopropyltrimethylammonium Chloride (MAPTAC)

Figure 2-5 Chemicals in photo-curable NIPAAm resin

N-isopropylacrylamide (also known as **NIPAAm**) is the monomer which has double bond. The monomer is the building block of long PNIPAAm chain structure.

N,N'-Methylene-bis(acrylamide) (also known as **BIS**) is the cross-linker that has two double bonds too. It can bind one polymer chain to another, resulting in PNIPAAm network structure.

Phenylbis (2,4,6-tri-methylbenzoyl) phosphine oxide is the photo initiator (PI) that can absorb photons and generate free radicals under light projection. The free radical can combine with the monomer molecule to form reactive molecule.

Sudan I is photo absorber (PA) which controls the penetration depth of the light. This is very important for layer-by-layer 3D printing method. The printing process of current layer should prevent its influence of light energy on the former printed layer. However, photo absorber will not be included in the photo-curable NIPAAm resin used in this chapter.

In addition, the transition temperature of temperature responsive hydrogel can be modified by copolymerizing with other types of monomer. For example, ionic monomer, which has hydrophilic side chain, is introduced to original polymer structure to enhance the hydrophilicity of network chains, realizing the shifting of transition temperature to higher temperature range [46]. In this thesis, we use **Methacrylamidopropyltrimethylammonium Chloride** (also known as **MAPTAC**) (*Sigma-Aldrich*) as the ionic monomer to be introduced. However, ionic monomer will not be included in the photo-curable NIPAAm resin used in this chapter.

Ethanol works as the solvent to dissolve all the chemicals mentioned above resulting in photo-curable NIPAAm resin.

2.2.2 Sample preparation

UV oven (*CL-1000, UVP*) provides 365 nm wavelength UV light which locates within the wavelength range that photo initiator has high level of absorption capability (2 weight % photo initiator in our photo-curable NIPAAm resin) as Fig. 2.5 shows.
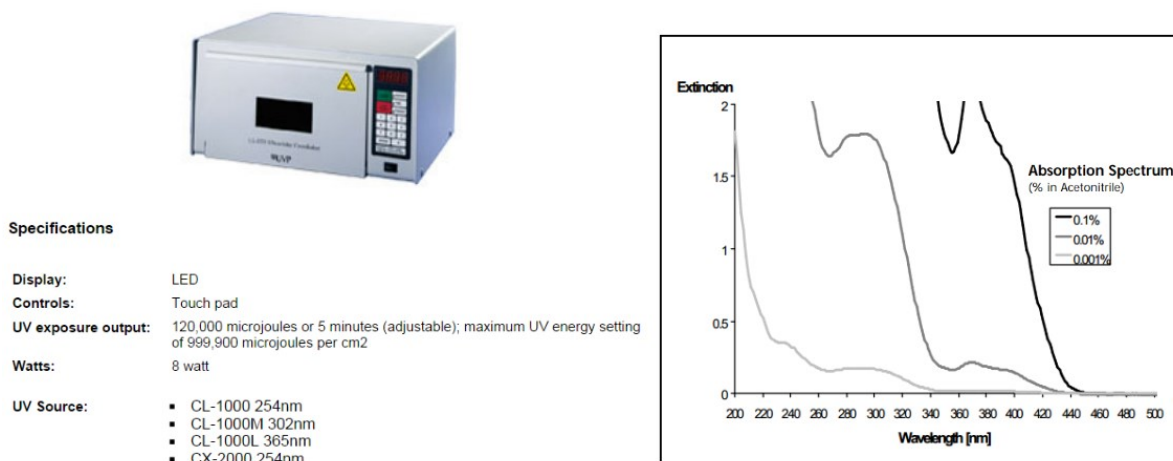
Figure 2-6 UV oven (left). Absorption spectrum of photo initiator, Phenylbis (2,4,6-tri-methylbenzoyl) phosphine oxide (right). Concentrations are expressed as weight % of solute in volume of the solvent

UV oven curing is used to fabricate fully cross-linked PNIPAAm sample by providing enough light energy to the photo-curable NIPAAm resin.

The NIPAAm resin is inserted in the sandwich-structure glass mold to fabricate thin film structure as Fig.2.6 and Fig 2.7 show. This glass mold has two 450-μm-thick spacers between two glass slides. Therefore, the thickness of thin film structure is 450 μm.

In order to obtain uniform cross-linking density within the thin film structure, flipping of sandwich-structure glass mold is needed after 1000 mJ cm^{-2} light energy dosage is projected on one surface of glass mold. Totally 2000 mJ cm^{-2} light energy dosage is given to fabricate the fully cross-linked 450-μm-thick PNIPAAm films.

Disk-shape samples, which are used as the experimental samples for temperature responsive property measurement, are punched by using manual punch tool (*Acuderm*). A Punch tool with 2.5 mm inner diameter is used. The actual size of punched disk-shape sample is measured again just after the sample being punched out the film to ensure the accuracy of following temperature responsive property measurement. This punched size is defined as the fabrication size of experimental sample.

Before the measurement, the disk shape samples are stored in DI water at room temperature for over 2 hours to remove the resin remaining in the structure and let the samples swell.

Add NIPAAm resin into sandwich structure glass mold

UV light

UV light

Sandwich structure

Flip the Sandwich structure

Sandwich structure

Punch the disk-shape samples

Store the samples in DI water
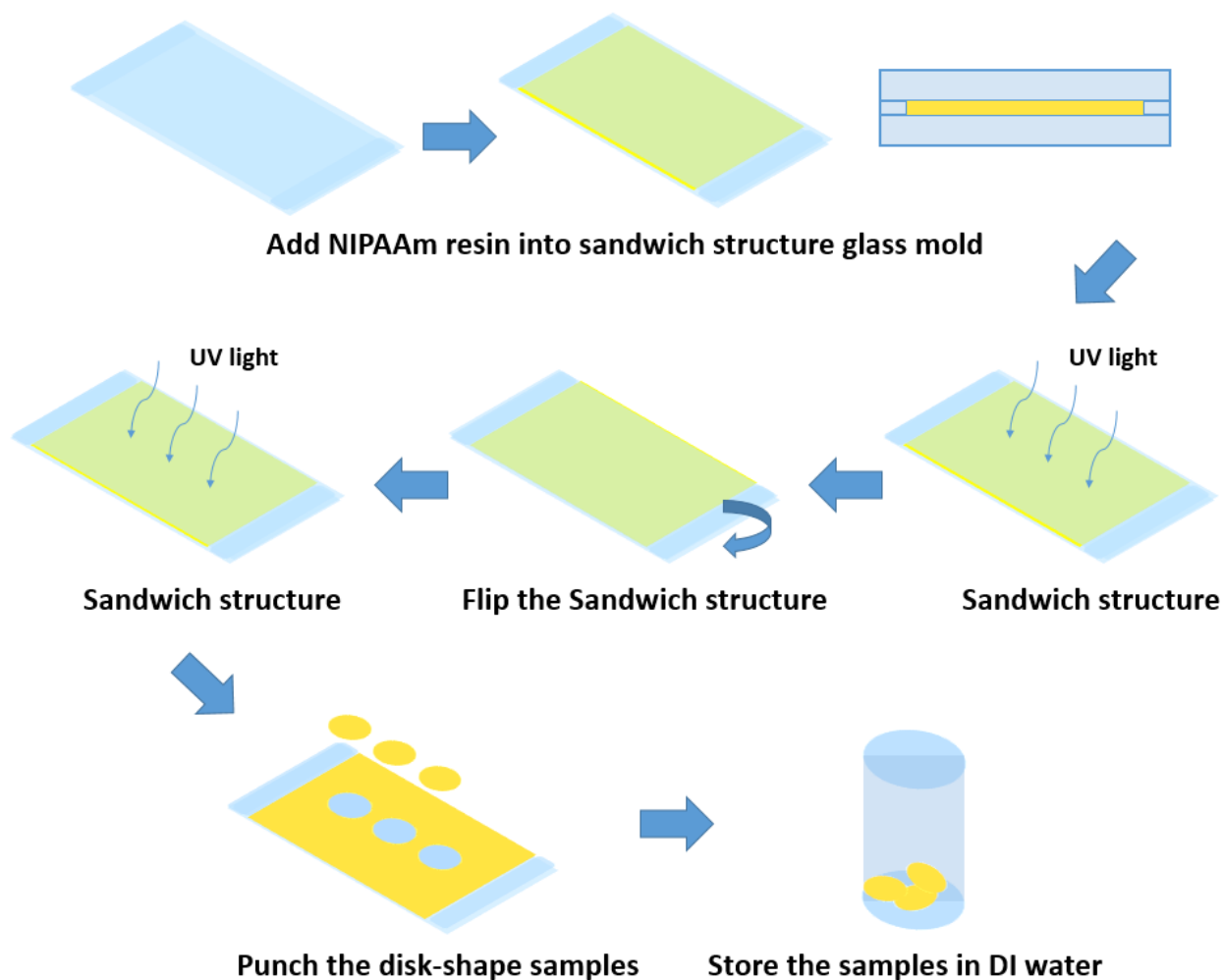
Figure 2-7 Schematic of samples preparation

Sandwich-structure glass
mold with NIPAAm resin

Cure

2.5mm

2.5mm punch tool

Punch
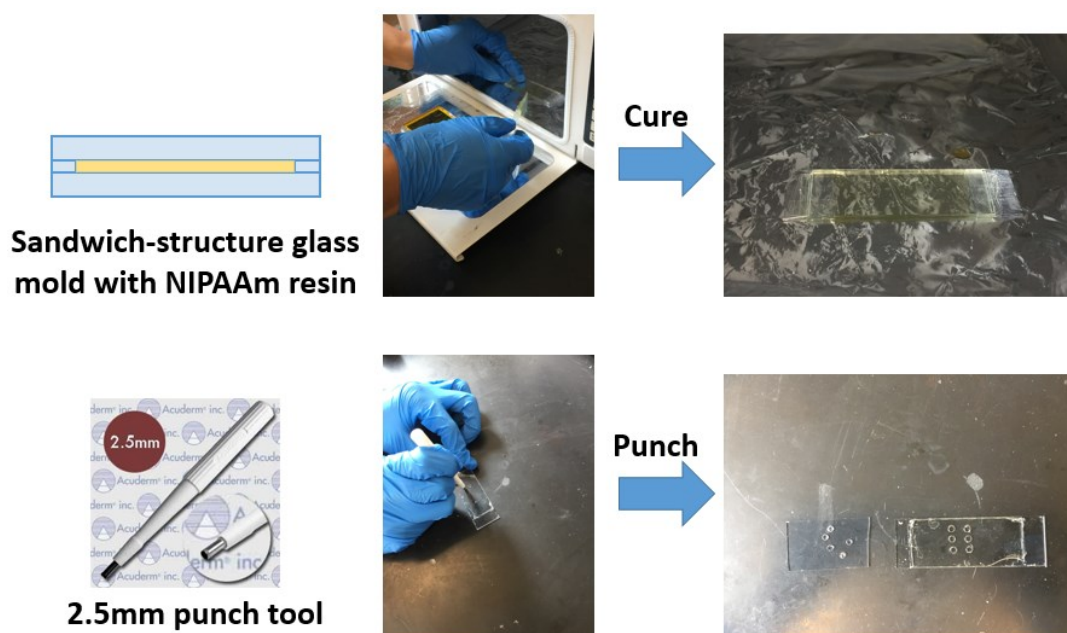
Figure 2-8 Actual images of Sandwich-structure glass mold, and cured samples

2.2.3 Measurement of temperature responsive swelling

To quantify the temperature responsive property of the PNIPAAm, the sizes of the disk-shape samples at different temperatures are measured and the swelling ratios at different temperatures are calculated.

2.2.3.1 Measurement system set-up

The temperature responsive property measurement system should be capable of precise temperature control and image recording. The measurement system used in this thesis consists of a refrigerated circulator (*SD07R-20, Polysciences*), a water bath (custom-built in machine shop), a digital camera (*Canon 5D*), data acquisition equipment (*National Instruments*) and a computer.

1. The refrigerated circulator provides precise and stable temperature control. Circulated water with certain temperature is continuously pumped out, and flows through the plastic pipe and the channel of custom-built water bath. Finally this circulated water returns back to circulator.

2. The custom-built water bath is made of heat-conductive metal aluminum. The water bath has a channel to let circulated water flow through and a sample chamber to store samples immersed in DI water. As heated water flows through the channel of the water bath, the heat will easily transfer from circulated water to metal to the DI water, and finally to the disk-shape PNIPAAm samples, which results in the shrinkage of the samples. Similarly, as the cooling water flows through the water bath, the heat will easily transfer from the DI water and the samples to the metal and finally to the circulated water, which results in the swelling of the samples. To prevent the evaporation of the DI water inside the chamber during the measurement process, especially the process at high temperature range, a transparent acrylic plate (*McMaster*) is covered on the top of the sample chamber and fastened by four screws. A thin polydimethylsiloxane (PDMS) film (*sylgard 184, Dow Corning*) located between the cover plate and the upper surface of water bath helps to seal the sample chamber.

3. The temperature measurement equipment consists of a K type thermocouple, NI-9211 module and NI cDAQ-9171 USB chassis. The measuring junction of the K type

thermocouple is inserted inside the sample chamber and two reference junctions are connect to the NI-9211 module. Then we insert NI-9211 module into cDAQ-9171 chassis and connect them to the computer. The voltage signals are measured and transferred to the temperature information. With built-in cold junction in NI-9211, high-accuracy temperature measurement can be achieved.

4. The camera is mounted on the top of the water bath to record the size of the samples at target temperature. Usually, a 5X objective lens is used to obtain good quality of sample images.
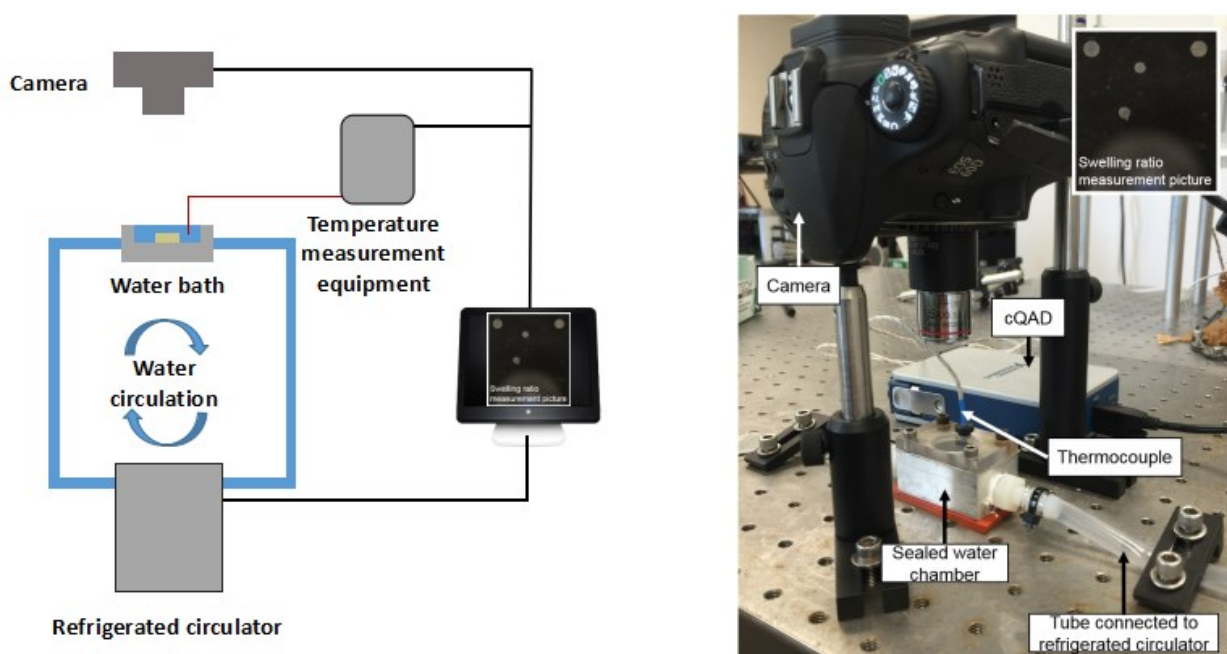
Figure 2-9 Schematic (left) and actual (right) image of measurement system

All the components of the measurement system are controlled by a LabVIEW code to execute automatic temperature change, temperature measurement and image recording. The logic of the LabVIEW code is shown below:
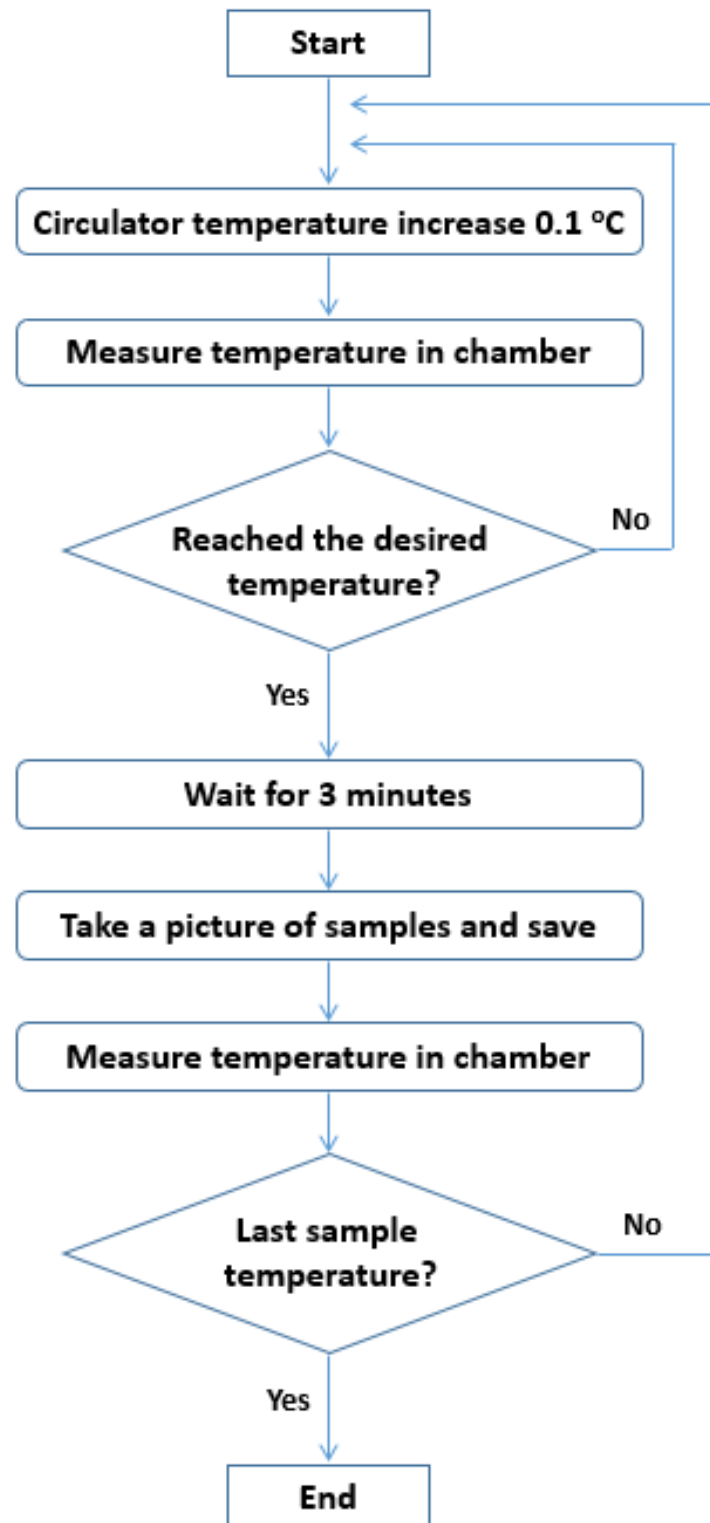
Figure 2-10 Flowchart of measurement process

The details of measurement process are described below:

This process begins at low temperature (lower than 10 ^{o}C within chamber).

Firstly, circulator begins to gradually increase the temperature at the rate of 0.1 ^{o}C per 25 seconds. The temperature in the sample chamber increase simultaneously but not at exactly a similar increasing rate. Therefore, thermocouple measures the temperature inside the chamber every time the circulator finishes 0.1 ^{o}C increment to get the precise temperature information. These two processes will repeat and stop temporarily once the temperature inside the chamber reaches the first sample temperature (we define that the measured temperature reaches sample temperature when the measured temperature is within Sample Temp. ± 0.1 ^{o}C). 3-minute waiting time is given to allow the samples to reach their equilibrium size around the sample temperature.

When the waiting time is up, the camera takes a picture of the samples and saves in the folder automatically. Besides, the temperature inside the chamber is measured again to precisely record the correspondent temperature of the samples in the picture which will be used for the swelling ratio measurement and calculation.

These processes above repeats in order when the following sample temperatures (every 5 ^{o}C after 10 ^{o}C) are reached.

Finally, the system automatically turns off when the sample image of last sample temperature (which is 50 ^{o}C when the measured samples are fabricated by resin without ionic monomer or 90 ^{o}C when the measured samples are fabricated by resin with ionic monomer) is taken. With all the images prepared, it is ready for the measurement process.

2.3.3.2 Sample size measurement

In this thesis, the definition of the swelling ratio is the ratio of the diameter of the disk shape sample at certain temperature to the diameter of fabrication size. When the swelling ratio equals to 1, the sample size equals to the fabrication size. If the swelling ratio is bigger than 1, the sample is considered as swollen. When the swelling ratio is smaller than 1, the sample is considered as shrunken.

We use image processing program (*ImageJ*) to measure the area of disk-shape sample in pixel^2 based on the images that are taken in the measurement process as Fig. 2.10 shows. Then we calculate the swelling ratio by the definition. After calculation, the swelling ratios

can be obtained and we create the swelling ratio vs. temperature plots (by *OriginPro*) to show the temperature responsive property of different types of sample.
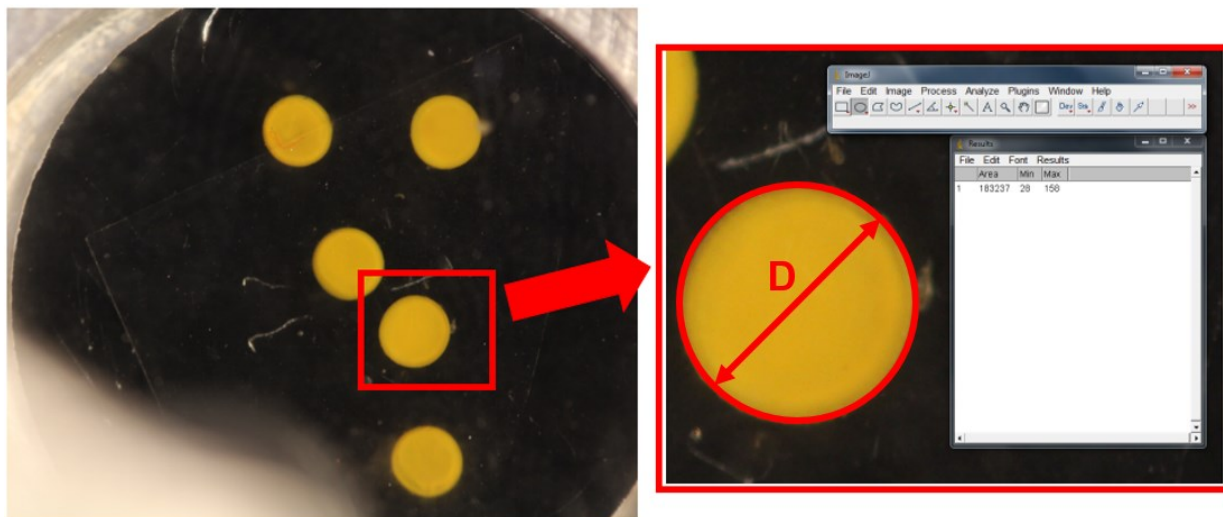
Figure 2-11 Measurement of swelling ratio of PNIPAAm samples

2.3.4 Sample weight measurement

The weights of PNIPAAm samples are also measured in dry condition and at low temperature to further investigate the temperature dependent swelling behavior.

We punch the samples using 6-mm punch tool out of different types of thin PNIPAAm films with similar thickness. We store the samples in the oven at 95 °C for over 2 hours before measuring the weights in dry condition. We immerse the samples in deionized water at 10 °C for over 2 hours and remove the water on the samples' surface by the paper towel before measuring the weights at low temperature condition.

2.4 Design of experiments

To study the principles of temperature dependent swelling, we designed two experiments to investigate the effects of molar ratio of NIPAAm monomer to cross-linker and concentration of chemical species in the solvent on temperature dependent swelling. We prepared two sets of photo-curable resins as shown in Table 2.1 and Table 2.2. Swelling ratio of all PNIPAAm

samples was measured at sample temperatures (10 °C, 15 °C, 20 °C, 25 °C, 30 °C, 35 °C, 40 °C, 45°C and 50 °C).

#	NIPAAm	Cross-linker	Molar Ratio	PI
1-1	6.2 M	65 mM	95.4	47.8 mM
1-2	6.2 M	130 mM	47.7	47.8 mM
1-3	6.2 M	195 mM	31.8	47.8 mM
1-4	6.2 M	259 mM	23.9	47.8 mM
1-5	6.2 M	324 mM	19.1	47.8 mM

Table 2-1 Chemicals concentration in photo-curable resin for first experiment

#	NIPAAm	Cross-linker	Molar Ratio	PI
2-1	2.6 M	136 mM	19.1	20.0 mM
2-2	4.4 M	230 mM	19.1	33.9 mM
2-3	6.2 M	324 mM	19.1	47.8 mM
2-4	8.0 M	419 mM	19.1	61.7 mM
2-5	9.7 M	508 mM	19.1	74.8 mM

Table 2-2 Chemicals concentration in photo-curable resin for second experiment

For the first experiment, the molar ratio of NIPAAm monomer to cross-linker is varied by changing the cross-linker concentration while the NIPAAm monomer concentration is kept constant (Resin 1-1 ~ 1-5). Since cross-linker concentration is much lower than that of NIPAAm monomer concentration, the volume of chemical species in the solvent remains almost constant. Therefore, the change of cross-linker concentration should have little effect

on the shrinkage at high temperature. On the other hand, with higher cross-linkers concentration, the length of PNIPAAm chains between cross-linking sites would decrease leading to reduced swelling size of PNIPAAm at low temperature.

For the second experiment, the concentrations of all chemical species in the solvent are varied at the same time while the molar ratio of NIPAAm monomer to cross-linker and the molar ratio of NIPAAm monomer to PI are kept constant (Resin 2-1 ~ 2-5). With higher NIPAAm monomer concentration in the resin, the concentration of chemical species increase results in larger volume of PNIPAAm network structure at high temperature. On the other hand, with the constant ratio of NIPAAm monomer to cross-linker, the length of PNIPAAm chains are kept constant leading to the constant swelling size of PNIPAAm at low temperature.

In addition, the weights of PNIPAAm samples are also measured in dry condition and at low temperature to further support the proposed principles.

The weights of PNIPAAm samples with different molar ratio of NIPAAm monomer to cross-linker (Resin 1-1, 1-3 and 1-5) are measured in dry condition and at low temperature to investigate the effect of molar ratio of NIPAAm monomer to cross-linker on swelling at low temperature.

The weights of PNIPAAm samples with fixed molar ratio of NIPAAm monomer to cross-linker but different concentration of chemical species in the solvent (Resin 2-1, 2-3 and 2-5) are measured in dry condition and at a low temperature to investigate the effect of density of molecules in NIPAAm photo-curable resin on shrinkage at high temperature.

2.5 Result and discussion
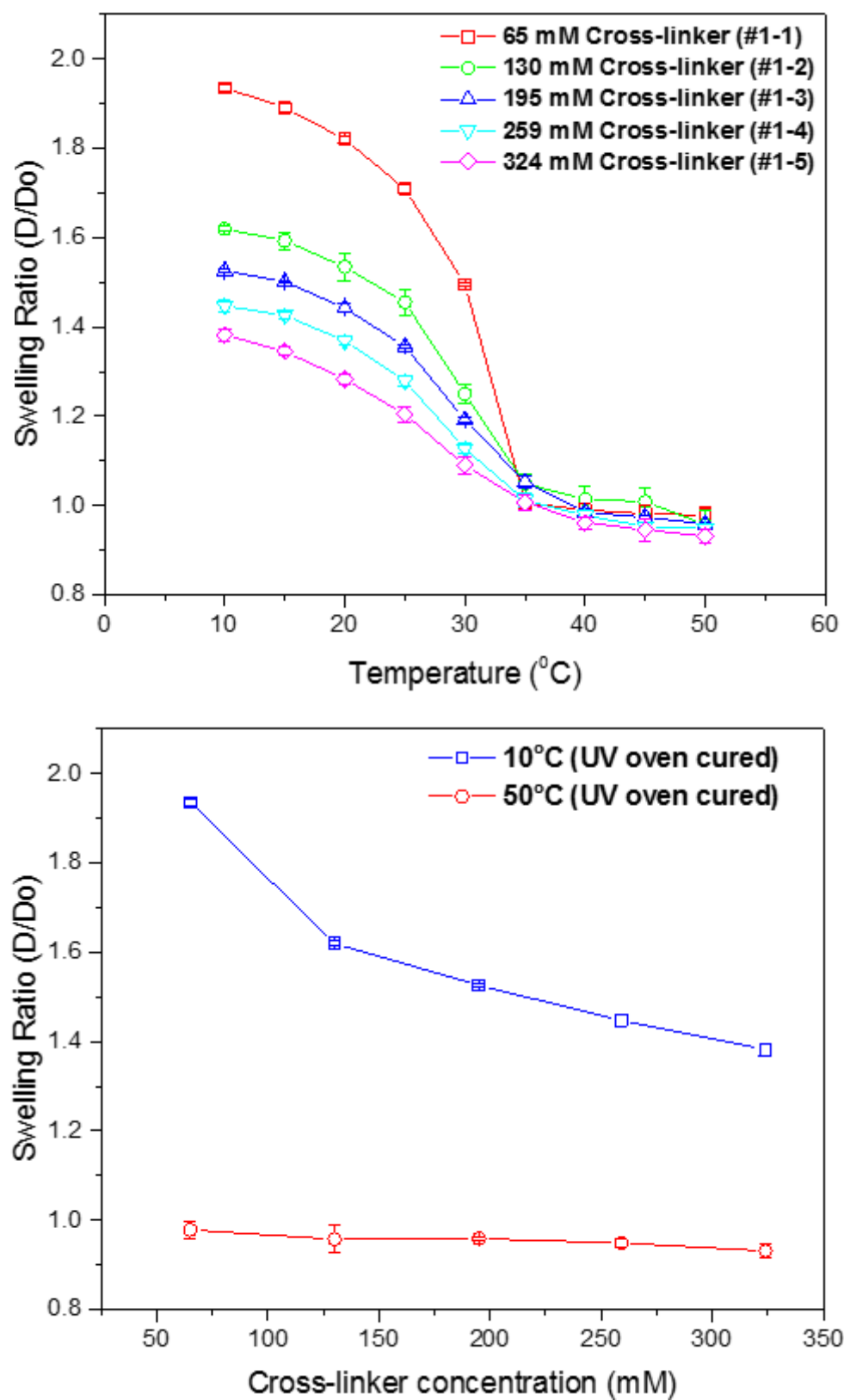
Figure 2-12 Effect of molar ratio between NIPAAm monomer and cross-linker on swelling behavior

Fig. 2.12 (top) shows the swelling ratios of samples with different molar ratio of NIPAAm monomer to cross-linker (different cross-linker concentration but constant NIPAAm monomer concentration) at all sample temperatures.

Firstly, the temperature responsive property is easily found. In low temperature range, all samples swell, with the swelling ratios bigger than 1. In high temperature range, all samples shrink, with the swelling ratios smaller than 1. The swelling ratio change sharply at around 35 °C, which indicates the transition temperature.

Secondly, swelling size of lower cross-linker concentration PNIPAAm sample at low temperature is bigger than that of higher cross-linker concentration PNIPAAm sample. However, when temperature increase the shrinkage sizes of all the samples are almost same. It is because the lower cross-linker concentration in NIPAAm resin leads to the lower stretchability when PNIPAAm swells at low temperature and the constant NIPAAm concentration results in the almost constant shrinkage size at high temperature.

Finally, if we extract the swelling ratio of samples with different cross-linker concentration only at the lowest and the highest sample temperatures to highlight this effect, we can get obtain Fig. 2.12 (bottom). The swelling ratio of samples made from 65 mM, 130 mM, 195 mM, 259 mM, and 324 mM cross-linker concentration resin is about 1.9, 1.6, 1.5, 1.45, and 1.4, respectively at the lowest temperature (10 °C, data points in blue color). However, all the swelling ratios of different samples are all about 0.9 at highest temperature (50 °C, data points in red color).

By changing a cross-linker concentration from 65 mM to 324 mM, almost 26 % of difference in swelling ratio can be achieved at 10 °C. However, there is no obvious swelling ratio difference at 50 °C. Therefore, the swelling at the low temperature is mainly determined by the molar ratio between NIPAAm monomer and cross-linker.
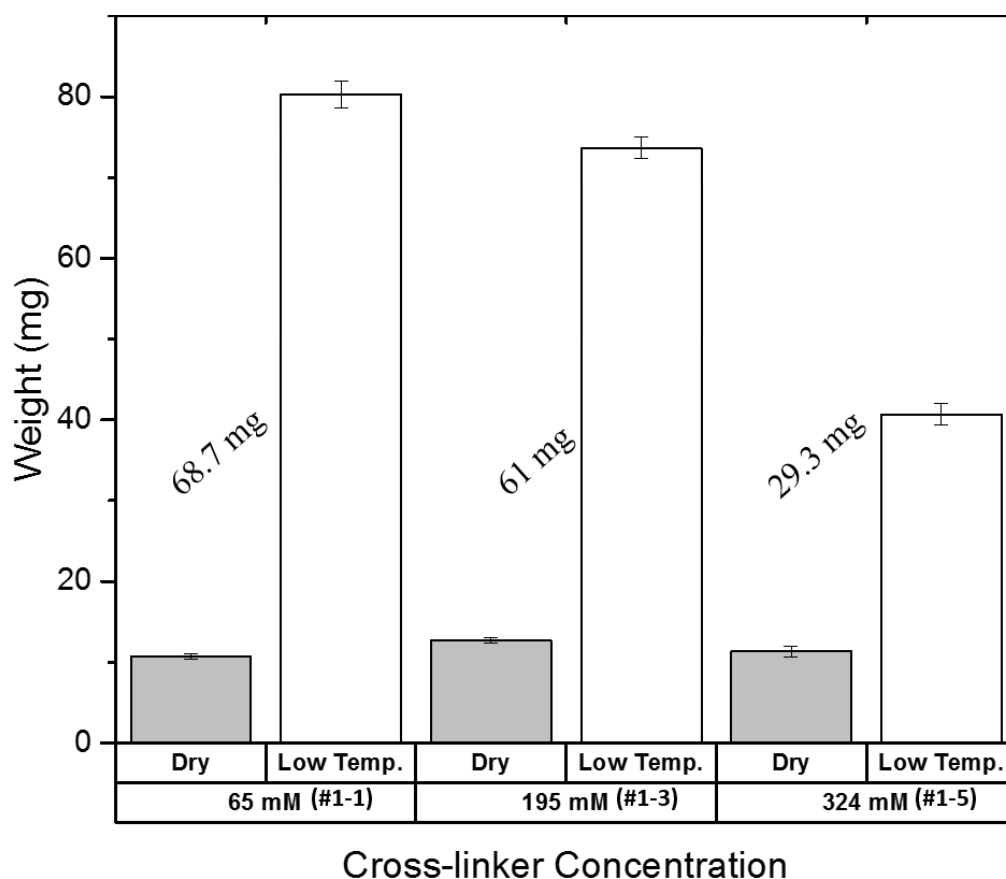
Figure 2-13 Weight of PNIPAAm with different molar ratio between NIPAAm monomer and cross-linker

The results of weight measurement are shown in Fig. 2.13. The numbers listed in plot are the weights of water contained in the samples at the low temperature.

In dry condition, the weights of PNIPAAm samples with different cross-linker concentration are almost the same because the constant concentration of NIPAAm in resin. Weights of different types of a sample at a high temperature have the similar condition as a dry condition because of the relative low water content.

At the low temperature, the weight of water molecules contained in high cross-linker concentration PNIPAAm sample is lighter than that contained in the low cross-linker concentration PNIPAAm sample because there is less water molecules being accommodated in lower stretchability PNIPAAm network.
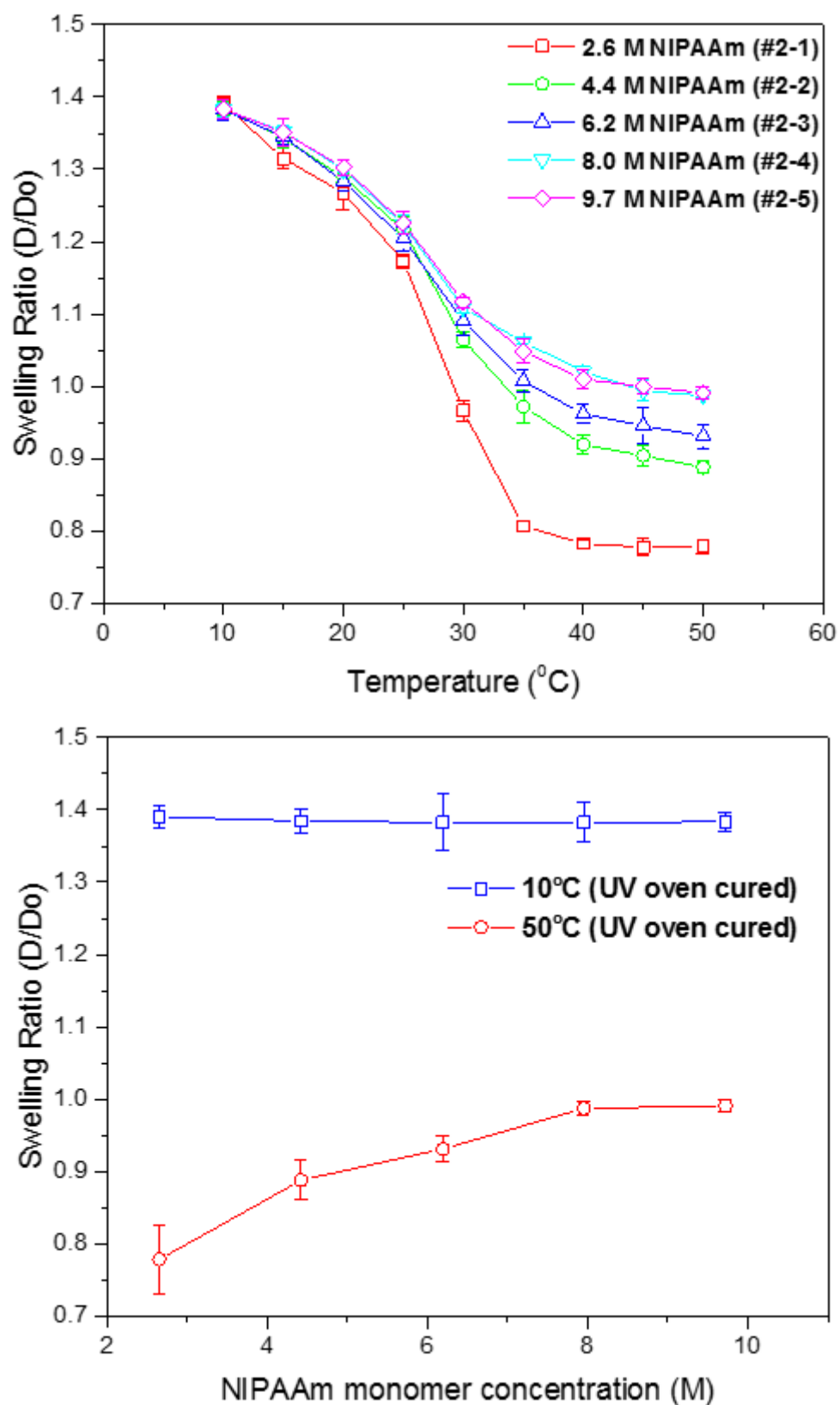
Figure 2-14 Effect of NIPAAm monomer concentration on swelling behavior of UV oven cured samples

Fig. 2.14 (top) shows the swelling ratios of the samples with different NIPAAm monomer concentration (different concentration of chemical species in the solvent but fixed molar ratio of NIPAAm monomer to cross-linker) at all sample temperatures.

Firstly, temperature responsive property is also easily found. In low temperature range, all samples swell, with the swelling ratios bigger than 1. In high temperature range, all samples shrink, with the swelling ratios smaller than 1. The swelling ratio change sharply at around 35 °C, which indicates the transition temperature.

Secondly, swelling size of lower NIPAAm concentration PNIPAAm sample at high temperature is smaller than that of higher NIPAAm concentration PNIPAAm sample. However, when temperature decrease the swelling sizes of all the samples are almost same. It is because the lower NIPAAm monomer concentration in NIPAAm resin leads to the less volume of PNIPAAm network and the fixed molar ratio of NIPAAm monomer to cross-linker results in the constant stretchability of network.

Finally, if we extract the swelling ratio of the sample with different NIPAAm monomer concentration only at lowest and highest sample temperatures, we can get Fig. 2.14 (bottom). All the swelling ratios of different samples are about 1.4 at lowest temperature (10 °C, data points in blue color), but the swelling ratio of the sample fabricated with 2.6 M, 4.4 M, 6.2 M, 8.0 M and 9.7 M NIPAAm monomer concentration resin is about 0.78, 0.90, 0.93, 0.97, and 0.99, respectively at highest temperature (50 °C, data points in red color).

By changing the NIPAAm monomer concentration from 2.6 M to 9.7 M, about 27 % of difference in the swelling ratio can be found at 50 °C. However, there is no obvious swelling ratio difference at 10 °C. Therefore, the shrinkage at high temperature molar is determined by concentration of chemical species in the solvent, or in other words, mainly determined by the concentration of NIPAAm monomer in the solvent.
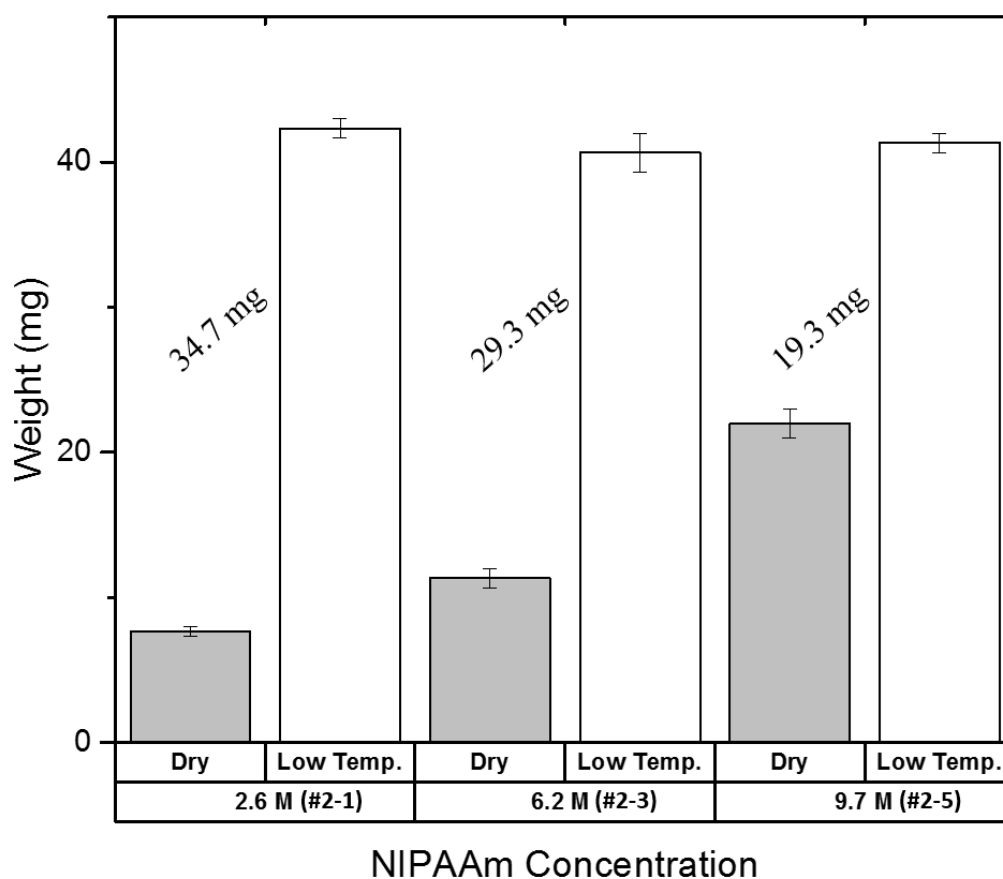
Figure 2-15 Weight of PNIPAAm with fixed ratio between NIPAAm monomer and cross-linker

The results of weight measurement are shown in Fig. 2.15. The numbers listed in plot are the weights of water contained in the samples at a low temperature.

In a dry condition, the weights of high NIPAAm monomer concentration PNIPAAm is greater than that of low NIPAAm monomer concentration PNIPAAm because the high concentration of NIPAAm in resin increases the weight of the PNIPAAm sample. Weights of different types of a sample at a high temperature have the similar condition as a dry condition because of the relative low water content.

At low temperature, the weight of water molecules contained in high NIPAAm monomer concentration PNIPAAm sample decrease because under the same stretchability condition of PNIPAAm network, less water molecules are able to be accommodated in higher density network.

2.6 Conclusion

In this chapter, we investigated the swelling of PNIPAAM at low temperature and shrinkage of PNIPAAm at a high temperature separately.

We hypothesized that the molar ratio of NIPAAm monomer to cross-linker in resin determines the swelling of PNIPAAm at a low temperature. We also hypothesized that the concentration of chemical species in the solvent determines the shrinkage of PNIPAAm at high temperature.

To prove our hypotheses, we prepared photo-curable NIPAAm resins with same NIPAAm monomer concentration but different molar ratio of NIPAAm monomer to cross-linker (namely, different cross-linker concentration) to fabricate the fully cross-linked PNIPAAm samples by using UV oven. After measuring their temperature dependent swelling ratios by using our custom-built measurement system, we found that these samples have different swelling size at low temperature but almost constant shrinkage size at high temperature. We also prepared the fully cross-linked PNIPAAm sample fabricated by UV oven using NIPAAm resins with different concentration of chemical species but same molar ratio of NIPAAm monomer to cross-linker and measure their temperature dependent swelling ratios. We found that these samples have almost constant swelling size at low temperature but different shrinkage size at high temperature.

Therefore, we found that we can independently control the swelling of PNIPAAm at low temperature by controlling the molar ratio of NIPAAm monomer to cross-linker and we can independently control the shrinkage of PNIPAAm at high temperature by controlling the concentration of chemical species in the solvent.

3. 3D printing of PNIPAAm

To fully control the temperature dependent swelling behavior of printed PNIPAAm sample, we have to fully understand the effects of different process parameters of PµSL fabrication method on temperature responsive property of the printed PNIPAAm sample.

Because of the characteristics of 3D printing method, we investigate the effects of both the chemical components and the printing process parameters on temperature dependent swelling of printed PNIPAAm sample.

We print a disk-shape sample using PµSL and measure the swelling ratio of samples at different temperatures using the same measurement system. We investigate the effects of molar ratio of NIPAAm monomer to cross-linker and concentration of chemical species in the solvent on swelling at low temperature and shrinkage at high temperature separately. We investigate the effect of ionic monomer on transition temperature change. We also investigate the effects of the printing process parameters of the PµSL system, such as gray scale of projection images and layer thickness, on temperature dependent swelling.

3.1 PµSL system

The layer-by-layer fabrication method can be applied to the photo-polymerization process of photo-curable NIPAAm resin.

3.1.1 PµSL system

Projection micro-stereolithography (PµSL) is a widely-used cost-effective 3D microstructure printing method that uses photo-polymerization process.

Our custom-built PµSL system consists of four major parts: optics part (UV light source, digital mask, a set of lenses and CCD camera), chamber part (sealed chamber which contains resin and capable of resin supply control), motion part (motorized translation stage) and control part (computer with LabVIEW codes).
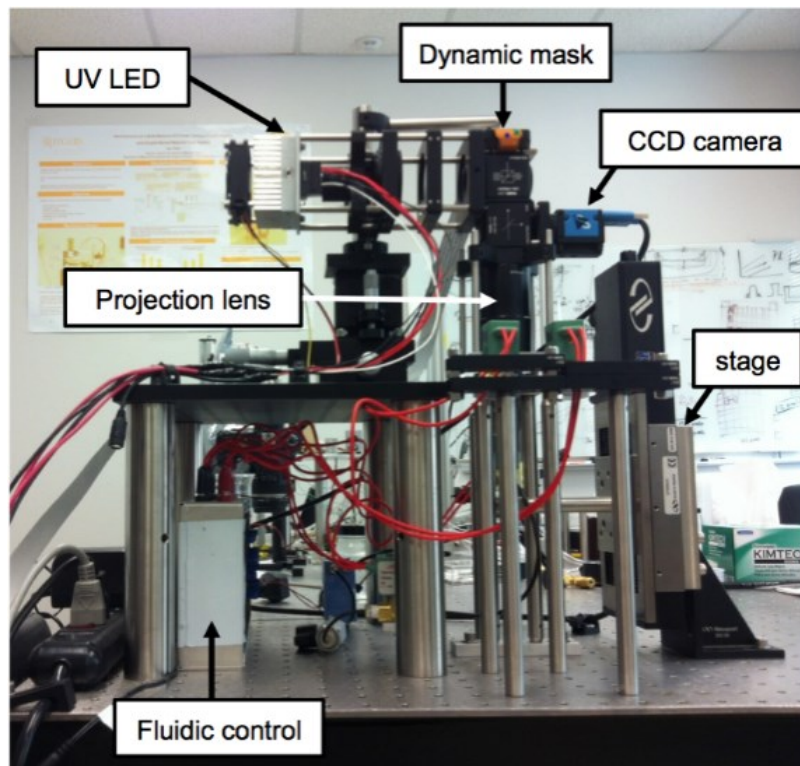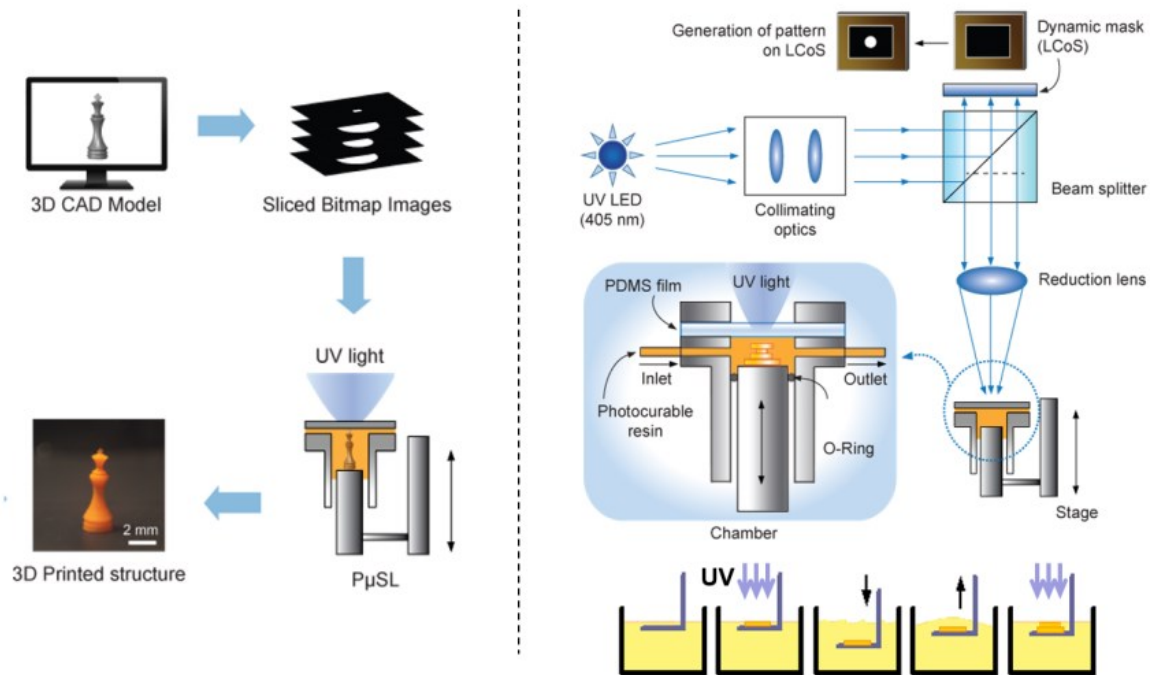
Figure 3-1 Schematic (up) and actual image (bottom) of PµSL system

Optics. UV LED is the light source (provides 365 nm wavelength UV light) for photo-polymerization. Light intensity can be controlled by a power supply, and the relationship between light intensity and current is shown in Fig. 3.2. LCoS chip works as a dynamic mask for 3D printing process. The patterned light for every layer is generated by LCoS chip based

on the respective BMP image. Therefore, light intensity can also be controlled by gray scale of BMP image, and the relationship between light intensity and gray scale is also shown in Fig. 3.2.
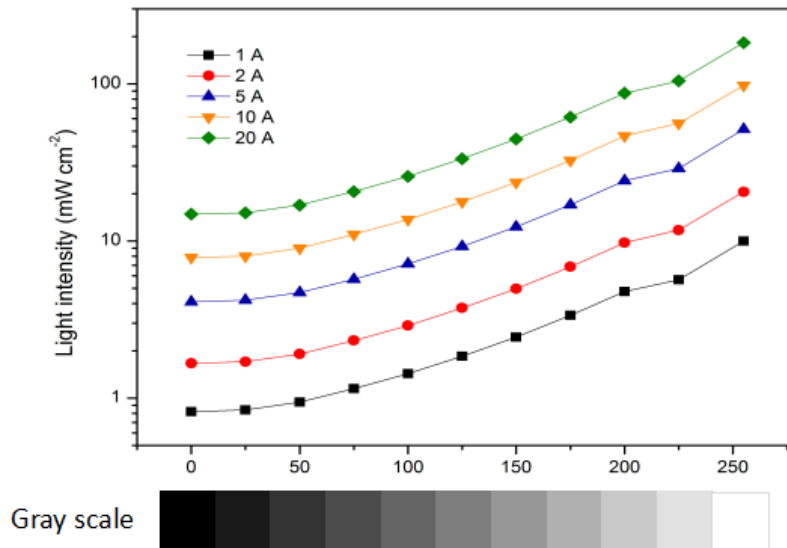
Figure 3-2 The relationship between light intensity and current or gray scale

After being reflected from dynamic mask, the patterned UV light is delivered to and focused on photo-curable resin for polymerization through a set of lenses, such as collimating optics, beam splitter and reduction lens. The resolution is 2.3 μm per pixel on the focal plane. CCD camera is used for visual feedback which is especially important for finding focal plane before printing process and checking fabrication quality of first several layers.

Chamber. The chamber part is the place where 3D polymer structure is printed. The chamber is covered and sealed by a PDMS membrane attached to a glass slide on the top.

The PDMS with glass slide is sandwiched by metallic components and fastened by four screws. The PDMS film provides the transparent enclosure for light transmission during structure fabrication process. A thin oxygen inhibition layer on the surface of PDMS film prevents the adhesion of printed structure to the surface of the film.

Sample plate is on the top of the piston where printed samples are located. This plate also helps to find the focal plane before the printing process to ensure the quality of printing. The piston can freely slide inside the cylindrical guide and is sealed by a rubber O ring.

The chamber also hosts input and output nozzles which are connected to inlet and outlet valve. The photo-curable resin is supplied from the resin bottle to the chamber through an input nozzle by gravity when the inlet valve is open and the piston moves downward. This resin supplement process will repeat after the printing process of every layer is finished and will stop when the whole printing process ends. When the piston moves upward and the outlet valve opens, the remaining resin is pushed out of the chamber through the output nozzle.
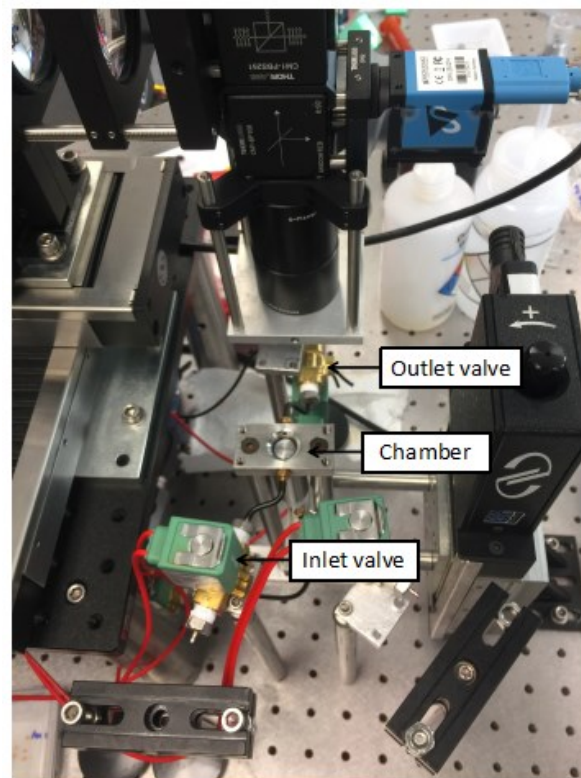
Figure 3-3 Details of PµSL system (optic part is moved out of printing position)

Stage. The movement of the sample holder (top of the piston) is controlled by motorized translation stage (*Newport*). The stage ensures layer-by-layer fabrication quality by providing precise layer thickness control.

Control part. The computer system not only operates the whole PµSL system in correct order by the LabVIEW codes, but also provides the necessary files such as BMP images and the process parameters for the printing process.

3.1.2 Printing process of PμSL system

Before the printing process beginning, the 3D model is designed by CAD software (*SolidWorks*) and sliced to a set of BMP images with an individual 2D layer pattern (by *Creation Workshop*). This set of BMP images together with the process parameters text file (including the number of layer, waiting time between layers, layer thickness and exposure time) will be sent to LabVIEW codes to control the 3D printing process.
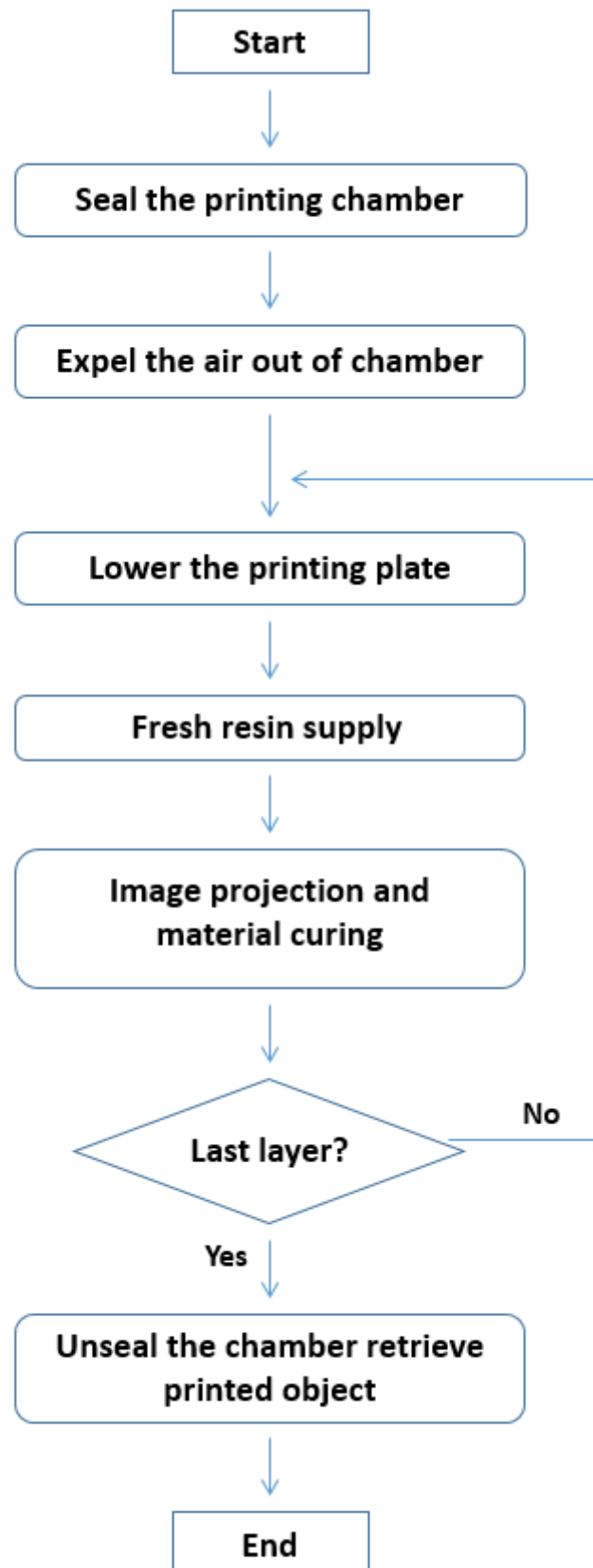
Figure 3-4 PμSL printing process
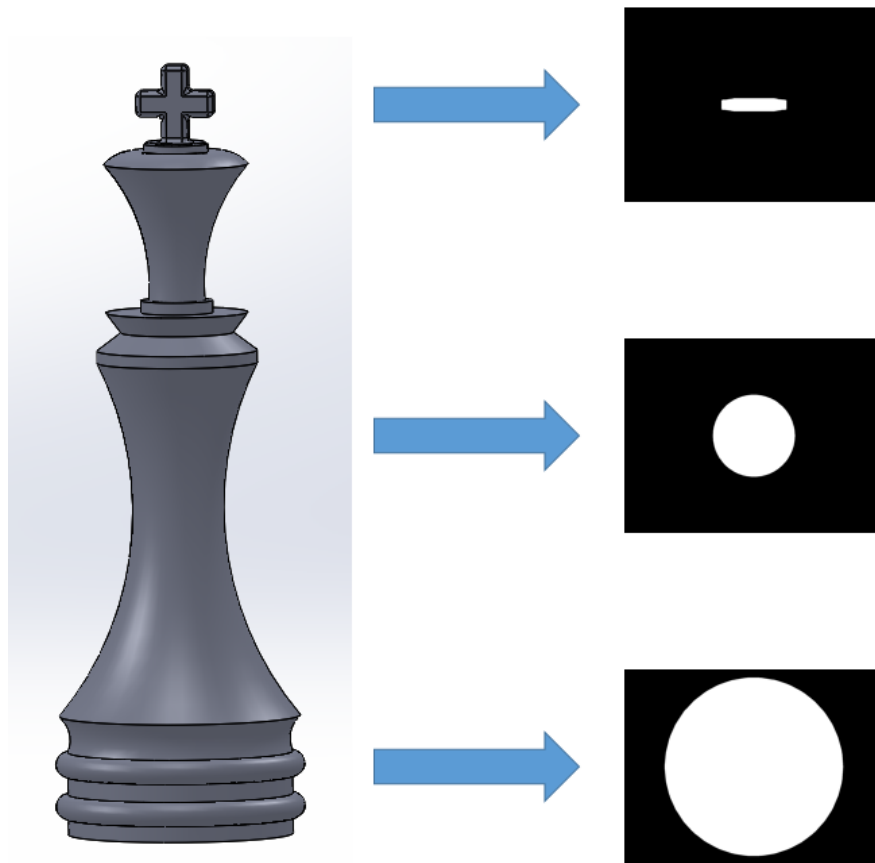
Figure 3-5 Example of modeling, slicing, BMP images and process parameter file

The printing chamber is sealed by covering a glass slide with PDMS membrane attached and fastened by four screws. To fill the printing chamber with curable resin and expel the air bubbles out of camber, the piston should move downward and upward together with the relevant valve open and irrelevant valve closed for several times. The sample plate finally contacts to the PDMS film when the filling process is done.

Optics move back to the top of the chamber once the resin supplying process is finished. After all the preparations are ready, the piston moves downward and the inlet valve opens simultaneously. Then the curable resin is supplied to the printing chamber. Once it stops at the designed position, the space for first layer is made.

The patterned light which is reflected from the dynamic mask is delivered through a set of lens and focused on the layer of the curable resin.

Once the first layer is fabricated, the piston lowers the sample plate where the printed structure rests to introduce fresh resin for the next layer. The next image of the layer is then

projected to cure the next layer on top of the printed layer. This process of the piston movement and the image projection is repeated during the fabrication of all the layers to complete the 3D structure.

Once the printing process is over, the glass slide is removed and the piston moves upward to let the printed structure be easily removed.

3.2 Effect of process parameters on swelling ratio of 3D printed PNIPAAm

PNIPAAm PµSL system printing process not only includes the photo-curable materials control but also the printing process control. These parameters can be used to tailor the swelling behaviors of 3D printed PNIPAAm.

All the swelling ratio test samples that are used for measurement are 3D printed in disk shape and we use the same swelling ratio measurement methods as we did in Chapter 2.

3.2.1 Effect of chemical components on swelling ratio

Based on the conclusion in Chapter 2, we want to independently control the swelling at the low temperature and the shrinkage at the high temperature in printed PNIPAAm hydrogel case too.

To show the possibility of this independent swelling behavior control, we designed two experiments to investigate the effects of molar ratio of NIPAAm monomer to cross-linker and density of NIPAAm in the resin on temperature dependent swelling of printed PNIPAAm hydrogel. We prepared two sets of photo-curable resins as shown in Table 3.1 and Table 3.3. In these resins, Sudan I (Sigma-Aldrich) is the photo absorber that controls the penetration depth of the light energy.

Swelling ratio of all PNIPAAm samples is measured at sample temperatures (10 °C and 50 °C). These swelling ratios of printed PNIPAAm hydrogels will be compared with that of PNIPAAm samples fabricated by UV oven.

For the fabrication of experimental samples, all the printing process parameters are listed in Table 3.2 and Table 3.4.

#	NIPAAm	Cross-linker	Molar Ratio	PI	PA
1-1	6.2 M	65 mM	95.4	47.8 mM	12 mM
1-2	6.2 M	130 mM	47.7	47.8 mM	12 mM
1-3	6.2 M	195 mM	31.8	47.8 mM	12 mM
1-4	6.2 M	259 mM	23.9	47.8 mM	12 mM
1-5	6.2 M	324 mM	19.1	47.8 mM	12 mM

Table 3-1 Chemicals concentration in photo-curable resin for first experiment

Light Intensity	Curing Time	Layer Thickness
2.4 mW cm^{-2}	10 Sec	30 μm

Table 3-2 Printing process parameters for resins in Table 3-1

#	NIPAAm	Cross-linker	Molar Ratio	PI	PA
2-1	2.6 M	136 mM	19.1	20.0 mM	12 mM
2-2	4.4 M	230 mM	19.1	33.9 mM	12 mM
2-3	6.2 M	324 mM	19.1	47.8 mM	12 mM
2-4	8.0 M	419 mM	19.1	61.7 mM	12 mM
2-5	9.7 M	508 mM	19.1	74.8 mM	12 mM

Table 3-3 Chemicals concentration in photo-curable resin for second experiment

Light Intensity	Curing Time	Layer Thickness

2.4 mW cm^{-2}	5~20 Sec	30 μm

Table 3-4 Printing process parameters for resins in Table 3-3

For the first experiment, the molar ratio of NIPAAm monomer to cross-linker is varied by changing the cross-linker concentration while the NIPAAm monomer concentration was kept constant (Resin 1-1 ~ 1-5). The shrinkage size at high temperature should remain almost constant while the swelling size at low temperature should be different.

For the second experiment, the concentrations of all chemical species in the solvent are varied while the molar ratio of NIPAAm monomer to cross-linker and the molar ratio of NIPAAm monomer to PI are kept constant (Resin 2-1 ~ 2-5). The shrinkage size at high temperature should be different while the swelling size at low temperature should remain almost constant.

As mentioned before, the transition temperature of PNIPAAm hydrogel can be shifted to higher temperature range by copolymerizing with ionic monomer, such as MAPTAC. To investigate the effect of the MAPTAC ionic monomer on transition temperature shifting, we prepared one set of photo-curable resins with different MAPTAC concentration as shown in Table 3.5. Swelling ratio of all PNIPAAm samples is measured at sample temperatures (from 10 °C to 85 °C with an increment of 5 °C).

For the fabrication of experimental samples, all the printing process parameters are the same as Table 3.2 shows.

#	NIPAAm	Cross-linker	Molar Ratio	PI	PA	MAPTAC

3-1	6.2 M	324 mM	19.1	47.8 mM	12 mM	0 M
3-2	6.2 M	324 mM	19.1	47.8 mM	12 mM	0.2 M
3-3	6.2 M	324 mM	19.1	47.8 mM	12 mM	0.4 M

Table 3-5 Chemicals concentration in photo-curable resin for transition temperature shifting experiment

For these experiments, higher concentration of MAPTAC ionic monomer concentration in resin leads to the increase in hydrophilicity of relative co-polymer. This results in the shifting of transition temperature to higher temperature range.

3.2.1.1 Effect of molar ratio of NIPAAm monomer to cross-linker
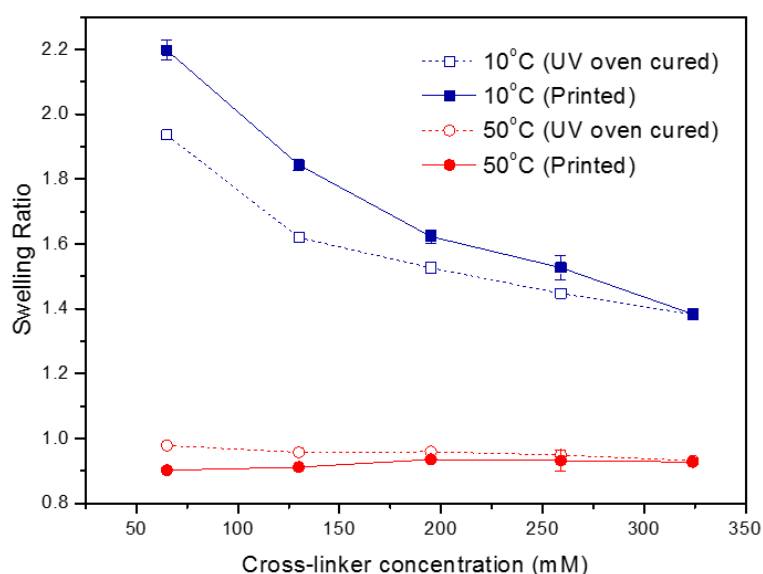
Figure 3-6 Effect of cross-linker concentration on swelling behavior of 3D printed samples

Fig. 3.6 shows the swelling ratio of sample with different cross-linker concentration at lowest and highest sample temperature. The open data points and dash lines show the swelling ratios of fully cross-linked samples fabricated by UV oven for comparison. The swelling ratio of sample made from 65 mM, 130 mM, 195 mM, 259 mM, and 324 mM cross-linker

concentration resin is about 2.2, 1.8, 1.6, 1.5, and 1.4, respectively at the lowest temperature (10 °C, solid data points in blue color). However, all the swelling ratios of different samples are about 0.9 at highest temperature (50 °C, solid data points in red color).

By changing a cross-linker concentration from 65 mM to 324 mM, almost 60 % of large difference in swelling ratio can be achieved at 10 °C. However, nearly no swelling ratio difference is shown at 50 °C.

Therefore, we can independently control the swelling at the low temperature by controlling the molar ratio of NIPAAm monomer to cross-linker and fixing NIPAAm monomer concentration in the solvent.

Compared to the results of fully cured samples fabricated by the UV oven, we find that there is a discrepancy between 3D printed samples and fully cured samples. The reason may be the samples are not fully cured under current printing process parameters. Though the difference exists, the tendency is the same.

3.2.1.2 Effect of concentration of chemical species in the solvent
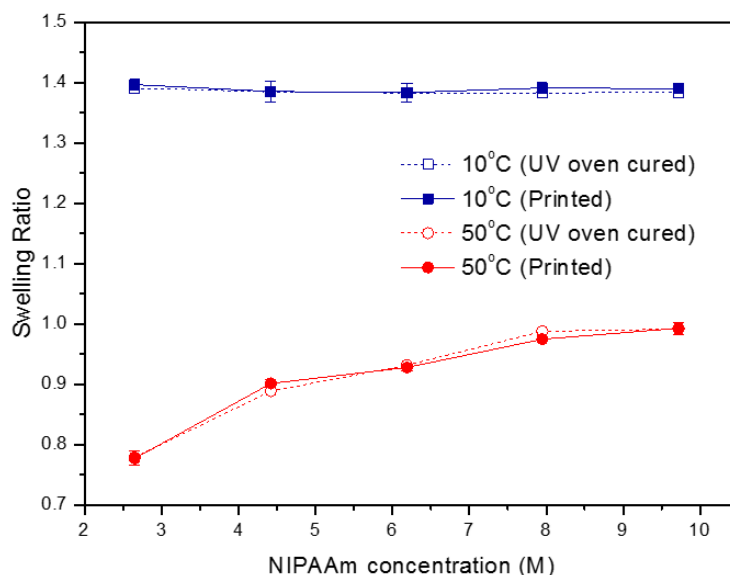
Figure 3-7 Effect of NIPAAm monomer concentration on swelling behavior of 3D printed samples

Fig. 3.7 shows the swelling ratio of a sample with different NIPAAm concentration at the lowest and the highest sample temperature. The open data points and dash lines show the

swelling ratios of cross-linked samples fabricated by UV oven for comparison. All the swelling ratios of different samples are about 1.4 at lowest temperature (10 °C, solid data points in blue color), but the swelling ratio of sample fabricated with 2.6 M, 4.4 M, 6.2 M, 8.0 M and 9.7 M NIPAAm monomer concentration resin is about 0.78, 0.90, 0.93, 0.97, and 0.99, respectively at highest temperature (50 °C, solid data points in red color).

By changing the NIPAAm monomer concentration from 2.6 M to 9.7 M, about 27 % of difference in the swelling ratio can be found at 50 °C. However, there is no obvious swelling ratio difference at 10 °C.

Therefore, we can independently control the shrinkage at high temperature by controlling the concentration of chemical species in the solvent and fixing the molar ratio of NIPAAm monomer to cross-linker.

Obviously, if these results are compared to the results of fully cured samples fabricated by UV oven, we find that we can achieve the similar swelling and shrinkage level in 3D printed PNIPAAm sample case.

### 3.2.1.3 Effect of ionic monomer concentration
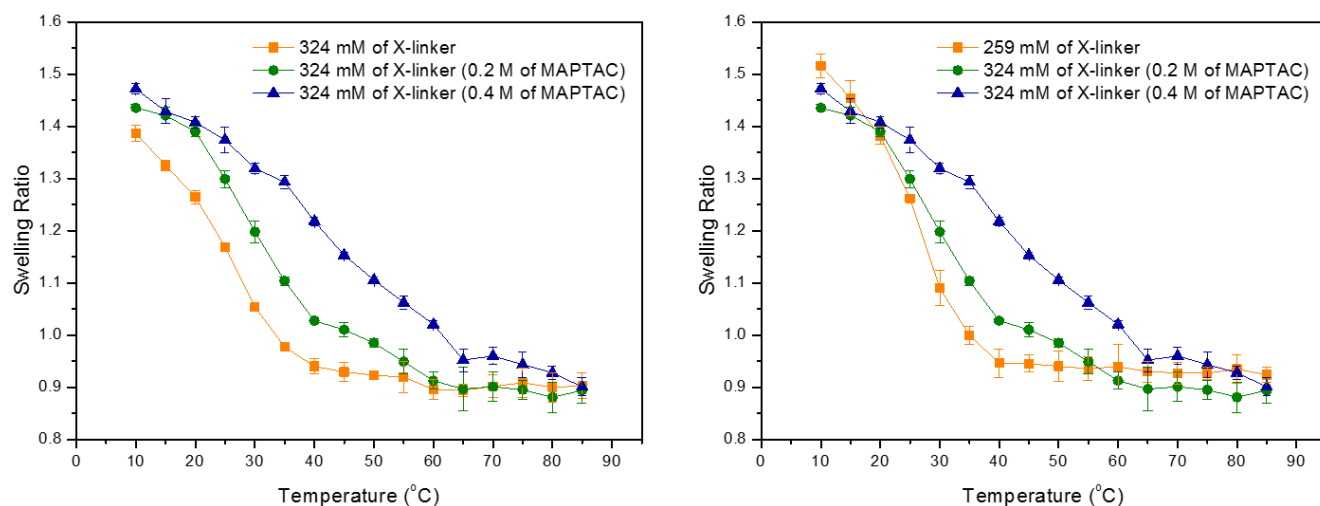
Figure 3-8 Effect of ionic monomer concentration on swelling behavior of 3D printed samples

Fig. 3.8 (left) shows the swelling ratio of the sample with different MAPTAC monomer concentration at sample temperature. The transition temperature of the sample made from 0.2

M and 0.4 M MAPTAC monomer concentration resin is shifted to a higher temperature which is about 45 °C (green line) and about 65 °C (blue line), respectively.

However, the existence of MAPTAC also increase the swelling ratio at a low temperature range because of the enhancement in hydrophilicity of network as shown in Fig 3.8. To decouple the changes of the swelling ratio at a low temperature range and the shifting of the transition temperature, PNIPAAm sample fabricated using lower cross-linker concentration is selected to make all the three plots (swelling ratios) overlap at both low and high temperature ranges as Fig. 3.8 (right) shown.

3.2.2 Effect of PµSL process parameters on swelling ratio

Thanks to the unique fabrication process of the PµSL system, printing process parameters such as light intensity and layer thickness can also be controlled to modify the swelling behavior.

Taking advantage of the usage of BMP images, light intensity can be modified by using different gray scale in BMP images as Fig. 3.2 shown.

With different level of light intensity and same exposure times, though photo-curable resin can all be perfectly printed in designed shape, cross-linking density is different among the PNIPAAm samples. The lower light intensity results in lower cross-linking density. However, higher light intensity results in higher cross-linking density. The cross-linking density change can lead to the swelling behavior change.

To find out the effect of gray scale of projection images on swelling behavior, we prepare one set of BMP images with different gray scale (namely light intensity) for printing PNIPAAm disk-shape samples as shown in Table 3.6. Photo-curable resin used in these experiments is listed in Table 3.7. Swelling ratios of all printed PNIPAAm samples are measured at the same sample temperatures (10 °C and 50 °C).

Sample #	Gray Scale	Light Intensity	Curing Time	Layer Thickness

1	**100**	**4.3 mW cm⁻²**	**4 Sec**	**30 μm**
2	**150**	**7.3 mW cm⁻²**	**4 Sec**	**30 μm**
3	**200**	**14.3 mW cm⁻²**	**4 Sec**	**30 μm**
4	**255**	**30.0 mW cm⁻²**	**4 Sec**	**30 μm**

Table 3-6 Gray scale and light intensity of BMP images

Resin #	NIPAAm	Cross-linker	PI	PA
4-1	6.2 M	324 mM	47.8 mM	12 mM

Table 3-7 Chemicals concentration in photo-curable resin for gray scale and layer thickness study

The layer thickness is the typical process parameter of the 3D printing method which can also be easily modified. During the printing process of one layer, the UV light is projected on the top part of the layer first and then penetrates into resin to a certain depth. Because of the photo absorber in resin, the light energy on the top part of a layer is higher than that of the bottom part. This leads to the difference of cross-linking density between top and bottom parts within one layer. Therefore, the cross-linking density on the top part is higher than that on the bottom part as Fig. 3.9 shown.

The thicker the layer thickness is, the larger the difference of cross-linking density between the top and the bottom parts. This may result in swelling behavior change at the high and the low temperature in both vertical and lateral directions.

To amplify the influence of the layer thickness and for the measurement convenience, rod structure is used instead of disk shape.
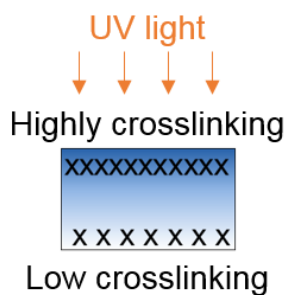
Figure 3-9 Difference of cross-linking density within one printing layer

To find out the effect of layer thickness on swelling behavior, we prepare one set of layer thickness parameters for printing the PNIPAAm rod structure samples as shown in Table 3.8. The swelling ratio of all types of PNIPAAm samples is measured at all sample temperatures (10 °C and 50 °C).

Sample #	Layer Thickness	Current	Curing Time
1	30 μm	3 A	9 Sec
2	60 μm	3 A	9 Sec
3	90 μm	3 A	9 Sec
4	120 μm	3 A	9 Sec
5	150 μm	3 A	9 Sec

Table 3-8 Layer thickness for rod structure

Similarly, photo-curable resin used in this study is listed in Table 3.7. Swelling behaviors in both lateral and vertical direction are studied.

3.2.2.1 Effect of gray scale of projection image
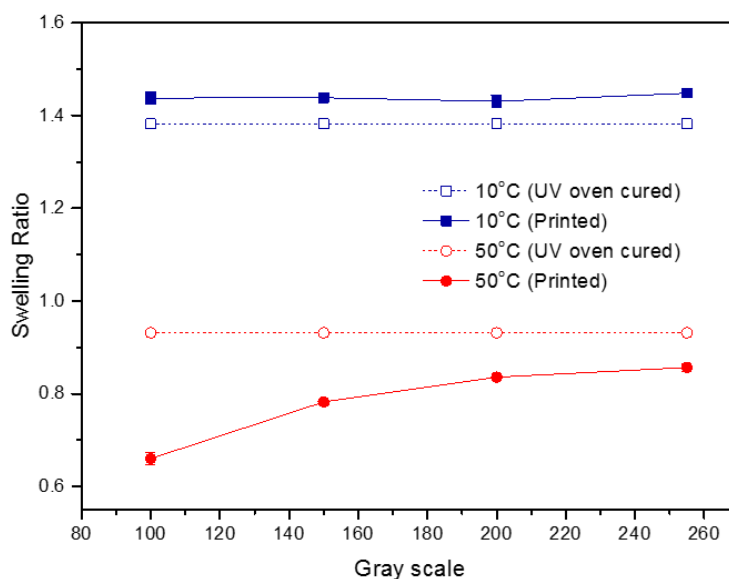
Figure 3-10 Effect of gray scale on swelling behavior of 3D printed samples

Fig.3.10 shows the swelling ratio of sample printed with BMP images of a different gray scale at the lowest or the highest sample temperature. The dash lines show the swelling ratios of fully cross-linked samples fabricated by UV oven for comparison.

All the swelling ratios of different samples are about 1.43 at lowest temperature (10 °C, solid data points in blue color), whereas the swelling ratio of the sample printed with BMP images of 100, 150, 200, and 255 gray scale is about 0.66, 0.78, 0.84, and 0.86, respectively at the highest temperature (50 °C, solid data points in red color). Obviously, lower light intensity (lower gray scale number) results in bigger swelling ratio difference between the lowest and the highest sample temperature.

Similar to the NIPAAm concentration study, by changing the gray scale from 100 to 255, about 30 % of the increase in the swelling ratio can be found at 50 °C. However, there is no influence on swelling at low temperature.

Therefore, we can independently control the shrinkage at high temperature by controlling the gray scale of projection images without the modification in concentration of chemical species. The advantage of this property is the capability of programming the swelling behavior within one layer.

3.2.2.2 Effect of layer thickness
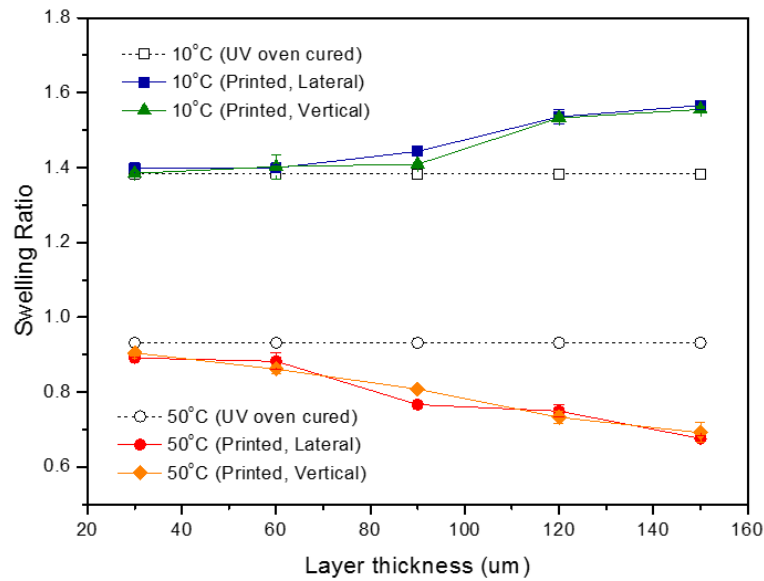
Figure 3-11 Effect of layer thickness on swelling behavior of 3D printed samples

Fig. 3.11 shows the lateral and vertical swelling ratio of sample printed with different layer thickness at lowest or highest sample temperature. The dashed lines show the swelling ratio of fully cured samples fabricated by UV oven for comparison.

In lateral direction, the lateral swelling ratio of the rod structure fabricated with 30, 60, 90, 120 and 150 µm layer thickness is about 1.40, 1.40, 1.44, 1.53 and 1.57, respectively at lowest sample temperature (10 °C, solid data points in blue color) and is about 0.89, 0.88, 0.77, 0.75 and 0.68, respectively at a highest sample temperature (50 °C, solid data points in red color). In vertical direction, the vertical swelling ratio of the rod structure fabricated with 30, 60, 90, 120 and 150 µm layer thickness is about 1.38, 1.40, 1.41, 1.53 and 1.56, respectively at lowest sample temperature (10 °C, solid data points in green color) and is about 0.90, 0.86, 0.77, 0.75 and 0.68, respectively at a highest sample temperature (50 °C, solid data points in orange color). Obviously, thicker layer thickness results in a larger swelling ratio difference between the highest and the lowest sample temperature both in the vertical and the lateral directions. By increasing the layer thickness from 30 to 150 µm, in both directions, approximately a 12 % increase in swelling at a low temperature and a 24 % decrease in the shrinkage at a high temperature, respectively.

Therefore, we can control the swelling behavior both at a low and a high temperature at the same time by controlling the layer thickness. Besides, the swelling behavior in the vertical direction is always identical to that in lateral direction during the changes of layer thickness, which suggests that the isotropic swelling behavior can be achieved.

3.3 3D printing of PNIPAAm micro-structures

We have done several studies on the effects of various process parameters on swelling behavior. Taking advantage of temperature responsive property of hydrogel and the capability of PμSL system, we can print a complex PNIPAAm micro structure for different applications. These applications will demonstrate our understanding of the PNIPAAm material and the PμSL system.

Here we introduce three demonstration models. Some of them needs the data collected in the former process parameter study of the 3D printed PNIPAAm samples.

3.3.1 Temperature dependent swelling of 3D printed micro-structure

As shown in Fig. 3.12, a chess piece is printed by PμSL system to show the reversible temperature responsive property of the printed sample.
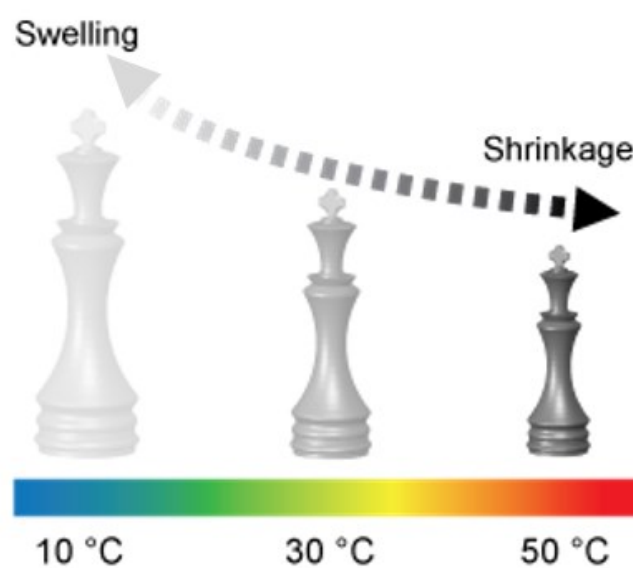
Figure 3-12 Schematic images of chess piece

The photo-curable resin for this chess piece is listed in Table 3.7 and the printing process parameters are listed in Table 3.2.

As Fig. 3.13 shows, we put the chess piece sample in deionized water and increase the temperature from 10 °C up to 50 °C, the chess piece shrinks. Then as we decrease the temperature from 50 °C back to 10 °C, the chess piece swells back to its former size. The plots show the time-dependent temperature change and the height of the chess piece at corresponding temperatures.
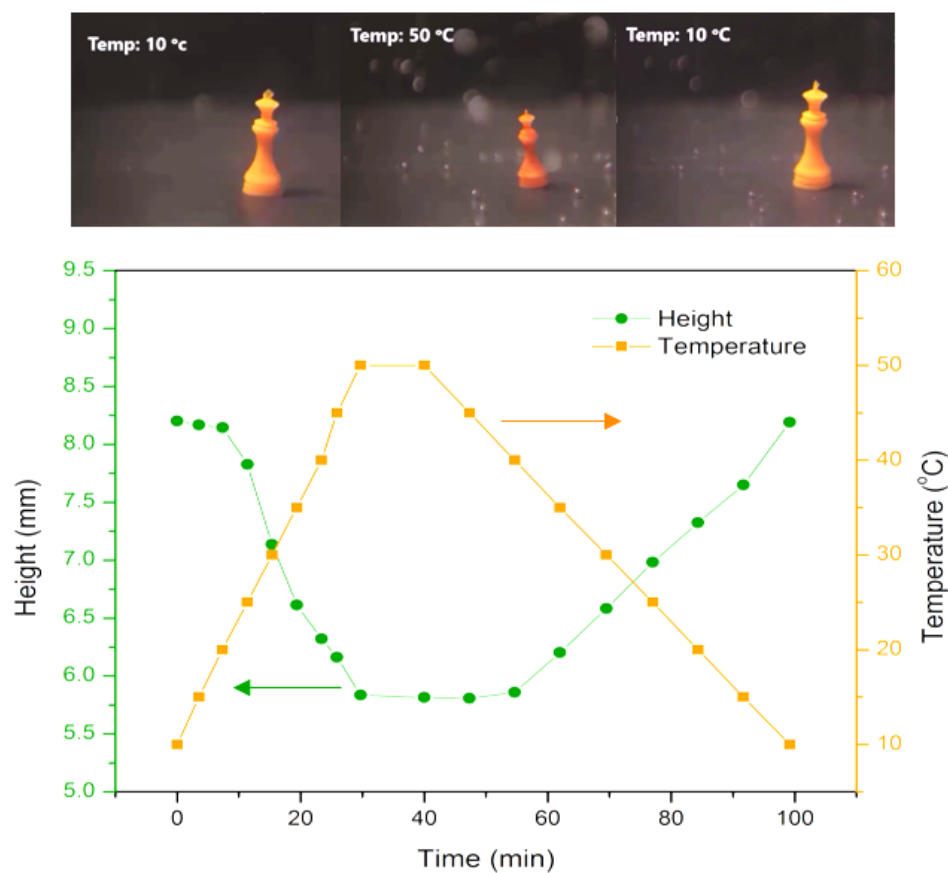
Figure 3-13 Reversible swelling of a 3D printed chess piece

3.3.2 Using gray scale to generate motion

As shown in Fig. 3.13, a gripper is printed by the PµSL system using the information of gray scale study.

To fabricate this gripper, the photo-curable resin is listed in Table 3.7 and the printing process parameters are listed in Table 3.6. Fingers of the gripper are 3D printed by a set of BMP images having two different gray scale parts, which are 100 (in gray color, inside) and 255 (in white color, outside), within one layer. Therefore, fingers of the gripper have two different swelling behavior parts.
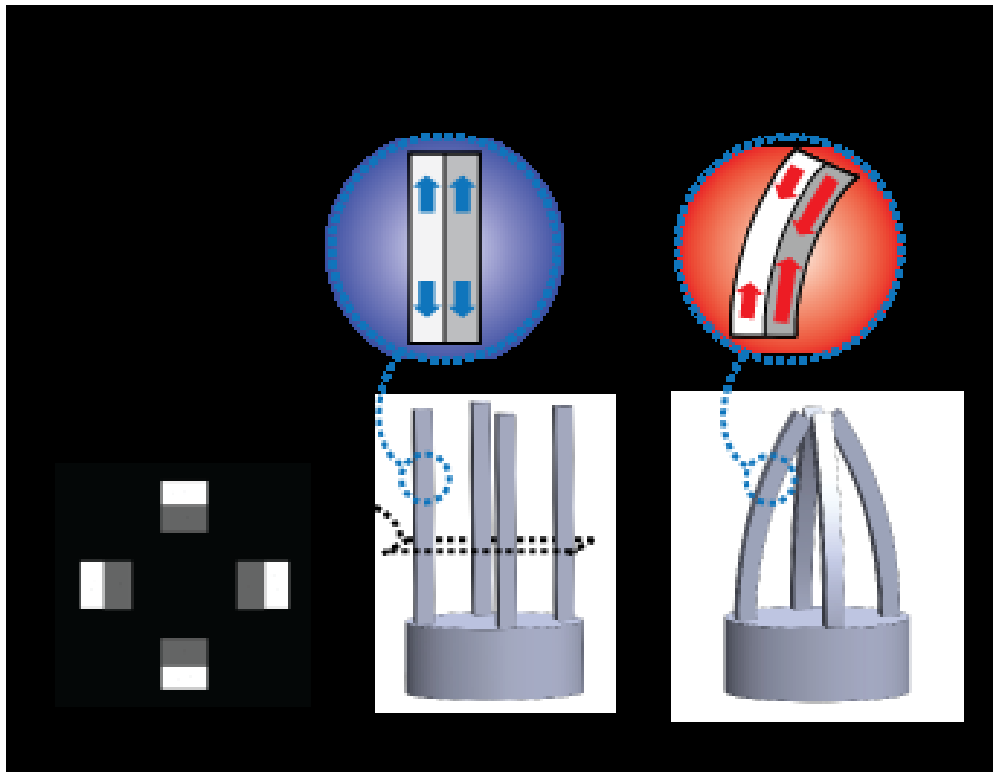
Figure 3-14 Schematic and BMP image of gripper

The temperature dependent swelling behavior of two gray scale parts are shown in plots in Fig 3.14 (green, 100 gray scale part; orange, 255 gray scale part).

The swelling ratio difference in several temperature ranges creates the strain mismatch between two parts. For example, in high temperature range (after 35 °C, as plots in Fig. 3.14 show), this mismatch results in bending of fingers toward inside because the inside part (100 gray scale) shrinks further than the outside part (255 gray scale). Below the transition temperature and in the low temperature range, the fingers swell without any bending motion since the inside and outside parts have the similar swelling behavior.

We put this PµSL printed micro gripper in deionized water and increase the temperature of deionized water from room temperature (around 28 °C) to 33 °C. At the beginning, the fingers remain almost straight because of the similar swelling ratio at that temperature. Then, as the temperature rises up, the fingers gradually bend toward inside (Fig. 3.13) because of the mismatch of swelling ratio.

This temperature controlled gripper, which can realize the gripping motion at a high temperature and release motion at a low temperature, may provide some ideas for the design of stimulus controlled micro scale soft robot.
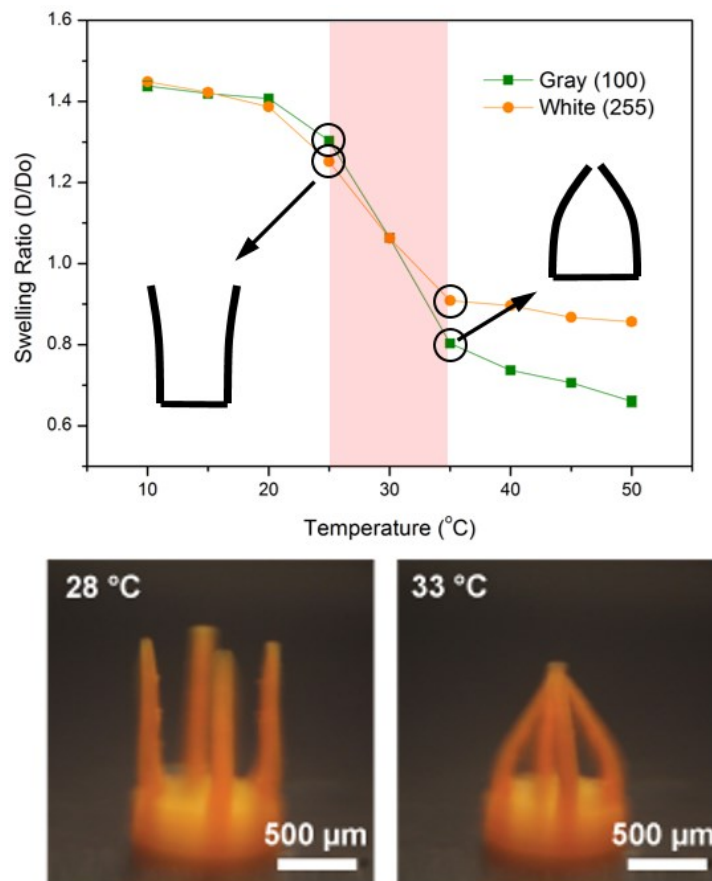
Figure 3-15 Experimental image of gripper

3.3.3 Using MAPTAC for multi-step deformation

As shown in Fig 3.15, a dumbbell is printed by the PµSL system using the information of ionic monomer study.

We use two different types of photo-curable resins to print a symmetrical dumbbell structure. One part (in orange color, Fig 3.15.a) is printed using the resin without any ionic monomer (the photo-curable resin # 3-1 in Table 3.5) which has normal transition temperature (around 32 °C, as orange plot in Fig 3.15.b shows). The other part (in blue color, Fig 3.15.a) is printed using the resin with 0.4 M MAPTAC ionic monomer (the photo-curable resin # 3-3 in Table 3.5) which has the higher transition temperature (around 45 °C, as blue plot in Fig 3.15.b shows). This dumbbell shows the reversible and non-uniform volumetric change as ambient temperature varies.
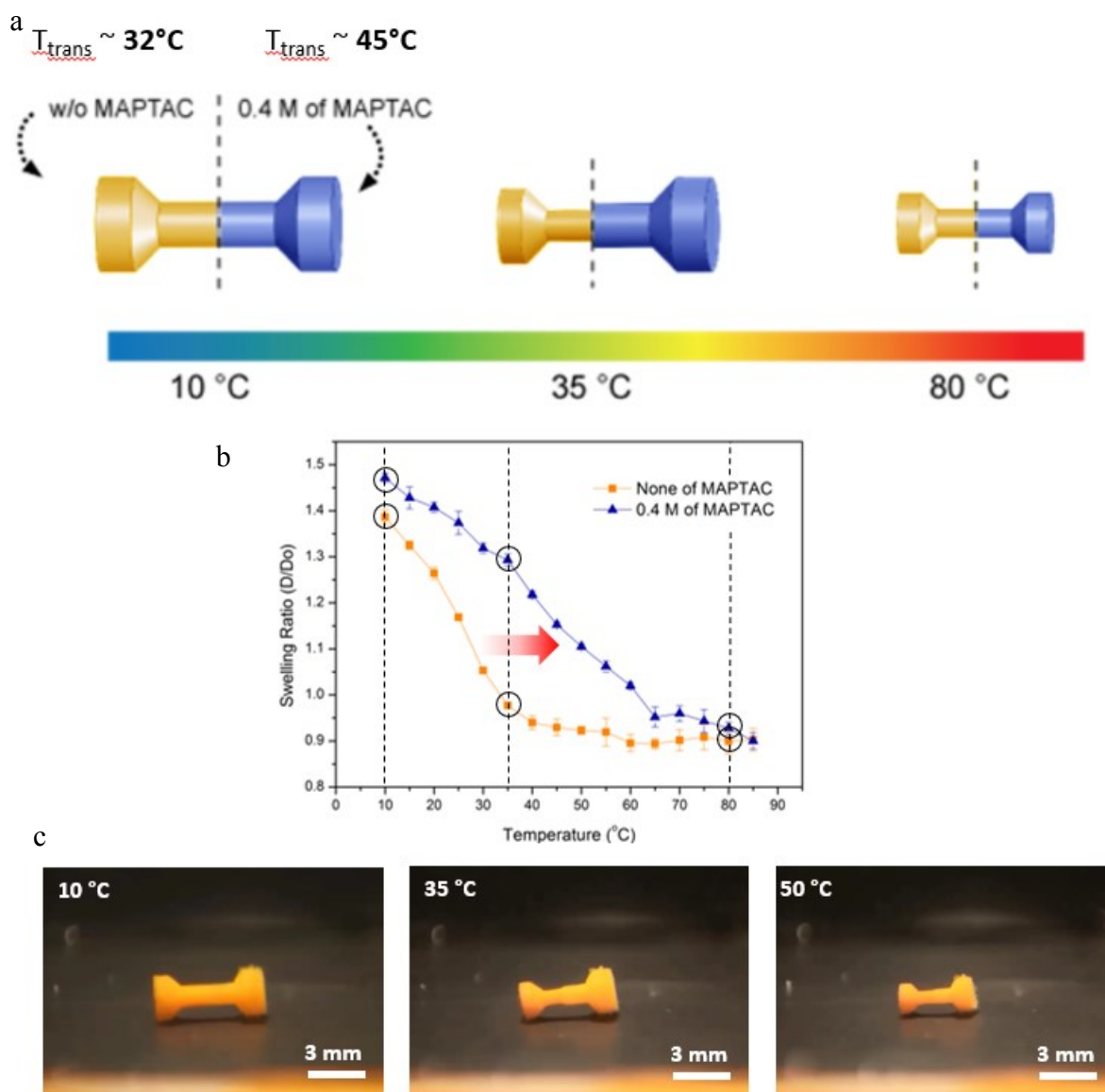
Figure 3-16 Schematic and experimental image of dumbbell

We put the PµSL printed dumbbell in deionized water and increase the temperature of deionized water from a low temperature (10 °C) directly to a high temperature (80 °C). Firstly, when the temperature increases from 10 °C to 35 °C, the left part printed using the resin without any ionic monomer shrinks obviously while the right part printed using the resin with ionic monomer does not show obvious shrinking phenomenon. Therefore, at 35 °C the left hand part is apparently smaller than the right hand side. Then, when we further increase the temperature from 35 °C to 80 °C, the left part printed using the resin without any ionic monomer shows the slight change but the right part shrinks obviously. Finally, at 80 °C, these two parts have equal size again (Fig 3.15.c).

3.4 Conclusion

In this chapter, we investigated the effects of different process parameters on the temperature responsive swelling property of the PµSL printed PNIPAAm sample.

We investigated the effects of chemical components on temperature dependent swelling behavior first. We kept the NIPAAm monomer concentration constant but change the molar ratio of NIPAAm monomer to cross-linker in resin (namely change the cross-linker concentration). The printed samples had the different swelling size at the low temperature but almost the same shrinkage size at high temperature. We can independently control the swelling at low temperature by controlling the molar ratio of NIPAAm monomer to cross-linker. We kept the molar ratio of NIPAAm monomer to cross-linker constant but change the NIPAAm monomer concentration in resin. The printed samples had almost the same swelling size at low temperature but different shrinkage size at high temperature. We can independently control the shrinkage at high temperature by controlling the concentration of the chemical species in the solvent.

We introduced the MAPTAC ionic monomer to investigate the shifting of the transition temperature. Higher MAPTAC concentration in the NIPAAm resin resulted in the shifting of the transition temperature of the printed PNIPAAm sample to a higher temperature range.

Then, we investigated the effects of the printing process parameters on the temperature dependent swelling behavior. We changed the gray scale of sliced projection images to investigate the effect of light intensity on the temperature dependent swelling behavior. We can also independently control the shrinkage at the high temperature by controlling the gray scale of projection images without the modification in chemical concentration.

We varied the layer thickness to investigate its effect on temperature dependent swelling behavior in both vertical and lateral directions. We can control swelling at low temperature and shrinkage at high temperature at the same level in both vertical and lateral directions by controlling the layer thickness.

Finally, based on all these findings, we fabricated several PµSL printed PNIPAAm micro-structures to demonstrate the ability to control the behaviors of printed sample by controlling the process parameters.

4. Improving mechanical property of PNIPAAm

One of the critical disadvantages of PNIPAAm hydrogel is its weak mechanical property. To apply the temperature responsive PNIPAAm hydrogel in more applications, improving its mechanical property while maintaining its temperature responsive property is important. We introduce ionically cross-linked alginate network into covalently cross-linked PNIPAAm network structure to fabricate PNIPAAm-alginate double-network hydrogel. The feasibility of this method is investigated by performing the tensile test and the swelling ratio test on PNIPAAm-alginate double-network hydrogel. Furthermore, the sequential cross-linking process is proposed to realize the 3D printing of the PNIPAAm-alginate double-network hydrogel with improved mechanical property.

4.1 Mechanical property of PNIPAAm

Although the PNIPAAm polymer like many other types of polymers have lots of potential applications, they always suffer from the limited mechanical behaviors such as softness and low stretchability.

This disadvantage may cause the unwanted failure in application such as unintended cell release and death for cell encapsulation [47], low durability of contact lenses [48] and PVA hydrogel-based artificial cartilage's insufficiency in strength, toughness, and friction properties for clinical tests [49]. Most hydrogels have a low stretchability; for example, alginate hydrogel rupture when stretched to only about 1.2 times its original length [50]. Most of the hydrogels are brittle with fracture energies of about 10 mJ^{-2} which is hundreds or a thousand times smaller than natural rubber [51].

4.2 Double-network tough hydrogel

Double-network hydrogel is a new type of material which can both have high water content and high mechanical strength and toughness. The reason for the improvement of mechanical strength and toughness is the introduction of energy-dissipating mechanisms [50]. Traditionally, a double-network gel where two networks (short chains and long chains) are

separately cross-linked by covalent bonds is used. When the gel is stretched, the short-chain network ruptures and dissipates energy. However, the rupture of the short-chain network causes permanent damage. Currently, the sacrificial covalent bonds are replaced by non-covalent bonds to realize recoverable energy-dissipating mechanisms. For example, when the covalent and ionic double-network gel is stretched, the ionic cross-link break and dissipate energy. The ionic cross-link then re-formed during a time interval after the first loading. Usually, synthesized double-network hydrogels possess hardness (elastic modulus of 0.1–1.0 MPa), strength (failure tensile nominal stress 1–10 MPa, strain 1000–2000%; failure compressive nominal stress 20–60 MPa, strain 90–95%), and toughness (tearing fracture energy of 100~1000 J m^{-2}) [52]. Therefore, creating a double-network structure in the original hydrogel network can be thought of as a method to improve the mechanical property of the original hydrogel while keeping its original hydrogel property.

Sun et al. mixed two types of cross-linked polymer: ionically cross-linked alginate, and covalently cross-linked polyacrylamide [50]. Within the double-network gel, ionic crosslinks between alginate and alginate are formed through Ca^{2+}, and covalent crosslinks between NIPAAm and NIPAAm are formed through cross-linker, and covalent crosslinks between NIPAAm and alginate are jointed by amine groups on PNIPAAm chains and carboxyl groups on alginate chains. The properties of this double-network hydrogel exceed those of either of its parent. It can be stretched to 20 times its original length without rupture. Its elastic modulus is 29 kPa, which is higher than the sum of the elastic moduli of the alginate and polyacrylamide gels (17 kPa and 8 kPa, respectively). The stress and the stretch at rupture were, respectively, 156 kPa and 23 for the hybrid gel, 3.7 kPa and 1.2 for the alginate gel, and 11 kPa and 6.6 for the polyacrylamide gel.

Wang et al. fabricated ion cross-linked calcium-alginate/poly(acrylamide) (PAAm) double-network hydrogels with excellent toughness and stiffness [53]. Within the double-network gel, ionic crosslinks between Alginate and Alginate are formed through Ca^{2+}, and covalent crosslinks between PAAm and PAAm are formed through cross-linker. The compressive strength of this double-network hydrogel is significantly improved by 92 % compared to

PAAm single network hydrogel, meanwhile the size and shape of calcium-alginate/PAAm

gel are not obviously changed and deformed, respectively.
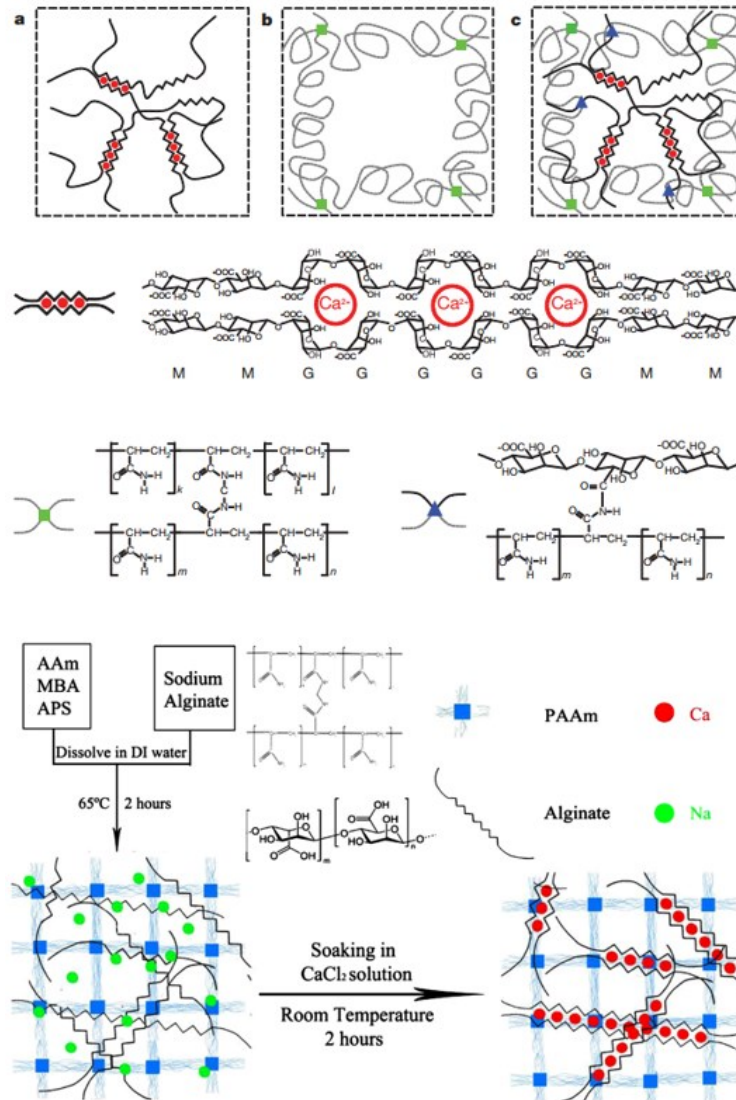
Figure 4-1 calcium-alginate/polyacrylamide double-network hydrogels(left) and calcium-alginate/poly(acrylamide) (PAAm) double-network hydrogels (right) [50] [53]

4.3 PNIPAAm Double-network hydrogel

We fabricate PNIPAAm-alginate Double-network hydrogel and investigate its capability of

keeping the original property of temperature responsive hydrogel and increasing the

mechanical property.

4.3.1 Design of experiment

To investigate whether this method can improve the mechanical property of the PNIPAAm hydrogel, we introduce ionically cross-linkable alginate to the PNIPAAm network. In this PNIPAAm-alginate double-network hydrogel network, ionic cross-links between Alginate and Alginate are formed through Ca^{2+} (ionic cross-linker); covalent cross-links between NIPAAm and NIPAAm are formed through BIS (covalent cross-linker). Besides, covalent cross-links between amine groups on the PNIPAAm chain and carboxyl groups on alginate chains are also formed by BIS.

We use the tensile test to investigate the mechanical property of the samples. Fig. 4.2 shows the custom-built tensile test system. The stress-strain curves of the PNIPAAm-alginate double-network hydrogel, covalent cross-linked PNIPAAm-alginate hydrogel and pure PNIPAAm hydrogel are measured and compared. Tensile modulus, strength, strain at break and toughness of these hydrogel samples are calculated and compared.

We also use the swelling ratio test to investigate whether the PNIPAAm-alginate double-network hydrogel is capable of keeping the original temperature responsive property of the PNIPAAm hydrogel. The test system is similar to what we use in Chapter 2.
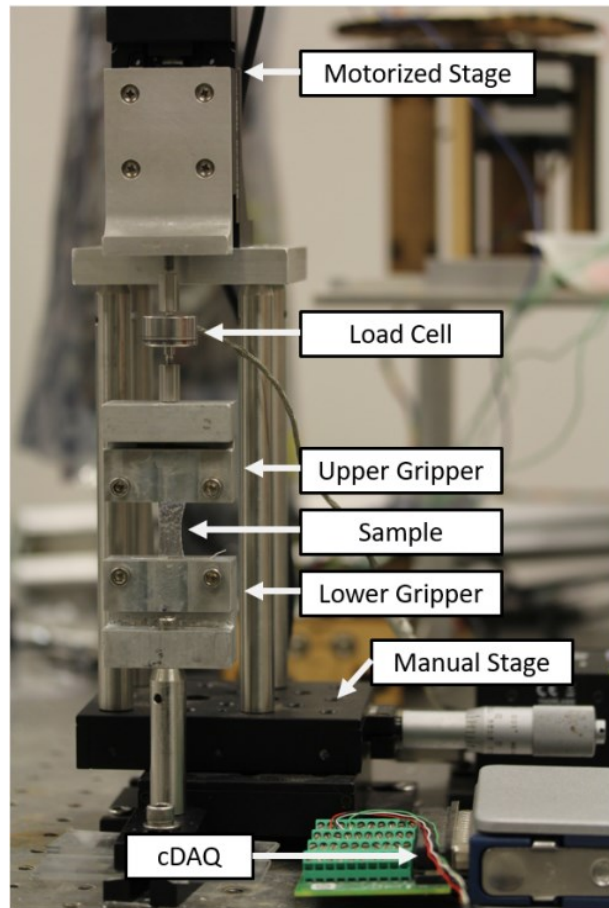
Figure 4-2 Tensile test system and measurement steps

4.3.2 Materials and sample preparation

We prepare the monomer solution, the cross-linker solution and the initiator solution separately firstly. Then mix all the solution together forming the covalent and ionic cross-links simultaneously to fabricate the PNIPAAm-alginate double-network hydrogel. The following tables show the chemical concentration of a different solution. The solvent for all solution is deionized water.

We prepare the $CaSO_4$ solution to introduce ionic cross-linker Ca^{2+} because the relatively slow cross-linking rate prevents the hydrogel from being fully cross-linked during the mixing process.

NIPAAm	Alginate	Weight Ratio (NIPAAm : Alginate)
0.91 M	0.013 g/mL	8 : 1

Table 4-1 Chemicals concentration in NIPAAm + Alginate solution

BIS
0.1 M

Table 4-2 Chemicals concentration in BIS (covalent cross-linker) solution

Ammonium Persulfate
0.2 M

Table 4-3 Chemicals concentration in photo initiator solution

CaSO$_4$
1.22 M

Table 4-4 Chemicals concentration in CaSO4 (ionic cross-linker) solution

The following steps show how we fabricate PNIPAAm-alginate double-network hydrogel for tensile test.

1. Clean two cylinders, Cylinder A and B, with DI water
2. Add NIPAAm + Alginate solution (10 mL) to Cylinder A

3. Add BIS solution (112.3 µL) to Cylinder A

4. Shake CaSO4 solution before using to make homogeneous solution

5. Add CaSO4 solution (140 µL) to Cylinder B

6. Add TEMED (33.3 µL) to Cylinder B

7. Add PI solution (216.7 µL) to Cylinder A

8. Remove the air from two cylinders

9. Connect two cylinders using the female luer coupler

10. Do piston action 50 times

11. Prepare the mold to make a shape

12. Pour the solution to mold

13. Store the mold for a day at room temperature

4.3.3 Results and discussion
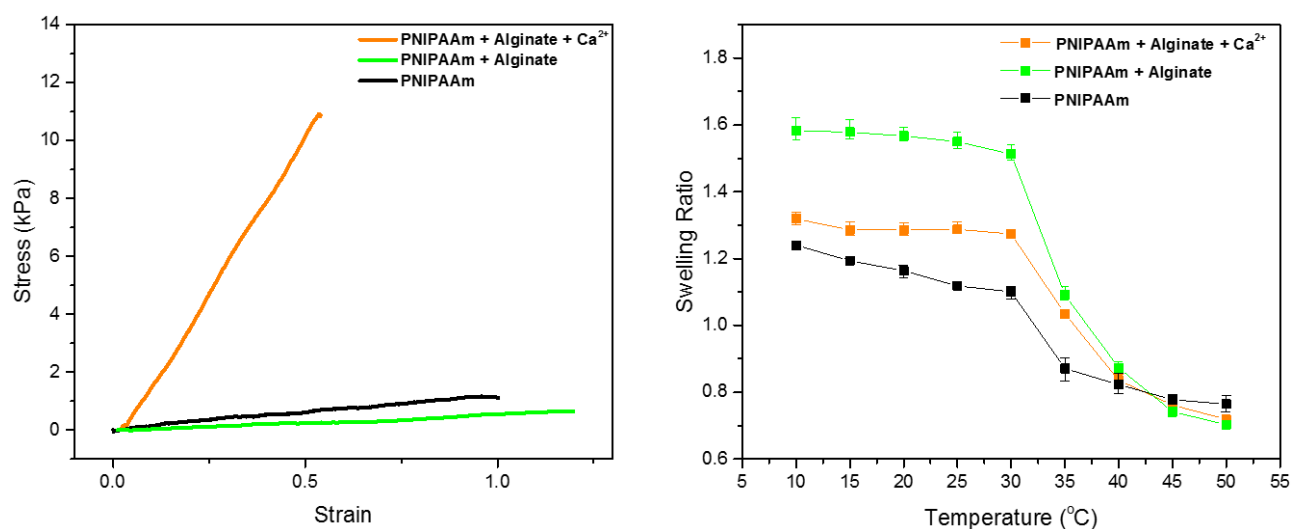
Figure 4-3 Mechanical property (left) and temperature responsive swelling behavior (right) of double-network tough hydrogel

The figure 4.3 (left) shows stress-strain curves of the PNIPAAm-alginate double-network hydrogel sample, covalently cross-linked PNIPAAm-alginate hydrogel sample and pure PNIPAAm hydrogel sample prepared using a fixed weight ratio between NIPAAm and Alginate. The quantitative analyses of mechanical properties of these samples have been

listed in the Table 4.5. Obviously, the double-network hydrogels have the improved mechanical property, which obtains higher modulus, higher strength and higher toughness. However, the stretchability is relatively decreased.

	Tensile Modulus (kPa)	Strength (kPa)	Strain at break	Toughness (J/m3)
PNIPAAm + Alginate + Ca^{2+}	18.4 ~ 21.5	10 ~ 10.8	54 % ~ 59 %	2,780 ~ 3,080
PNIPAAm + Alginate	~ 0.6	~ 0.65	~ 120%	~ 350
Pure PNIPAAm	~ 1	~ 1	~ 100 %	~ 600

Table 4-5 mechanical properties of different types of sample

Fig. 4.3 (right) shows the swelling ratio test results. PNIPAAm-alginate double-network hydrogel maintains the temperature responsive property of original PNIPAAm hydrogel. It swells at the low temperature and shrinks at the high temperature. The transition temperature is around 30 °C ~ 35 °C. Compared to pure PNIPAAm, tough hydrogel swells further at the low temperature. This may be attributed to the introduction of the hydrophilic alginate network.

4.4 Sequential cross-linking process

Previously, we fabricate the PNIPAAm-alginate double-network tough hydrogel sample by mixing monomer, the covalent and the ionic cross-linkers and the initiator together to initiate covalent and ionic cross-linking processes simultaneously. We found the improvement in mechanical property of double network hydrogel.

However, this fabrication method cannot be used in PµSL process because ionic cross-linking process begins once Ca^{2+} is added into resin. In order to realize the 3D printing of double-network hydrogel, we have to separate the covalent and ionic cross-linking process and cross-link them in order.

4.4.1 Design of experiment

We sequentially cross-link the PNIPAAm-alginate double-network hydrogel as Fig. 4.4 shows.

Before the cross-linking process, we prepare the evenly mixed NIPAAm + Alginate solution. During the cross-linking process, covalently cross-linking process is performed first. Covalent cross-links between NIPAAm and NIPAAm and between NIPAAm and Alginate are formed through BIS (covalent cross-linker). Therefore, polymer can be cured (3D printed) in the designed structure first.

Material preparation

Curing (3D printing)

Post-processing

NIPAAm/Alginate solution

Photo-polymerization
(Covalent crosslinking)

Enhancement of mechanical
property by introducing Ca^{2+}
(Ionic crosslinking)
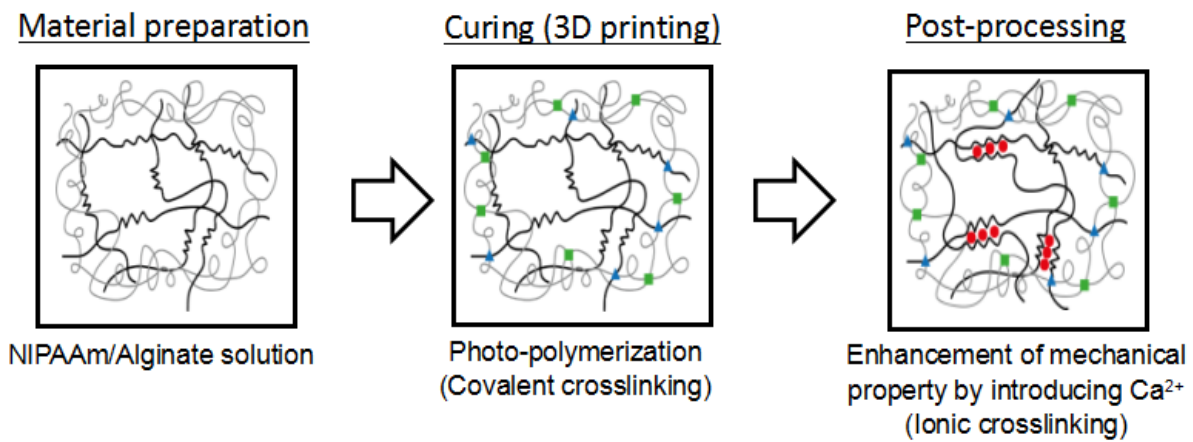
Figure 4-4 sequential cross-linking of covalent-ionic double-network PNIPAAm hydrogel

Then the ionic cross-linking process is introduced in the existed covalently cross-linked structure. In this post-processing procedure, ionic cross-links between Alginate and Alginate are formed through Ca^{2+} (ionic cross-linker). Therefore, the mechanical property of the cured structure is enhanced.

4.4.2 Materials and sample preparation

Based on this idea, we fabricate the samples using the same materials as 4.3.2 listed. However, we prepare $CaCl_2$ solution to introduce ionic cross-linker Ca^{2+} instead to minimize the post-processing time.

CaCL$_2$
1.5 M

Table 4-6 Chemicals concentration in CaCl$_2$ solution

The following steps show how we fabricate PNIPAAm-alginate double-network hydrogel for tensile test using sequential cross-linking process.

1. Clean two cylinders, Cylinder A and B, with DI water
2. Add NIPAAm + Alginate solution (10 mL) to Cylinder A
3. Add BIS solution (112.3 µL) to Cylinder A
4. Add TEMED (33.3 µL) to Cylinder B
5. Add PI solution (216.7 µL) to Cylinder A
6. Remove the air from two cylinders
7. Connect two cylinders using the female luer coupler
8. Do piston action 50 times
9. Prepare the mold to make a shape
10. Pour the solution to mold
11. Store the mold for a day at room temperature
12. Soak the cured samples in $CaCl_2$ solution for a day at room temperature

4.4.3 Results and discussion
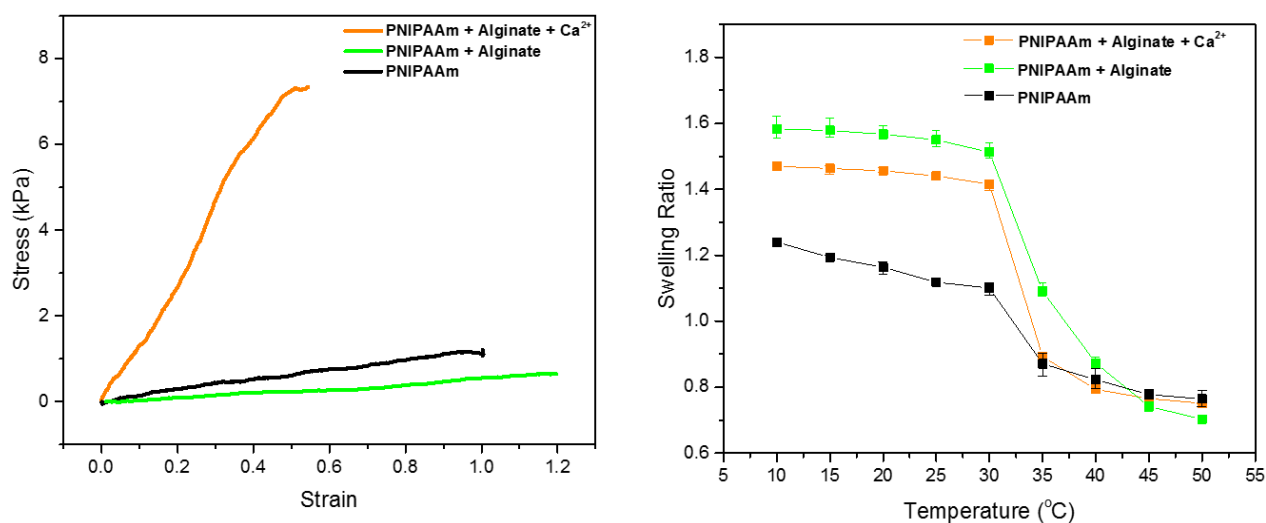
Figure 4-5 Mechanical property (left) and temperature responsive swelling behavior (right) of sequential cross-linked double-network hydrogel

The figure 4.5 (left) shows the stress-strain curves of sequentially cross-linked PNIPAAm-alginate double-network hydrogel sample, covalently cross-linked PNIPAAm-alginate hydrogel sample and pure PNIPAAm hydrogel sample. The quantitative analyses of mechanical properties of these samples have been listed in the Table 4.7. The sequentially cross-linked double-network hydrogel clearly shows the improved mechanical properties, which obtain higher modulus, higher strength and higher toughness. Still, by comparison with pure PNIPAAm hydrogel, the sequential cross-linked double-network hydrogel shows decreased stretchability.

Fig. 4.5 (right) show the swelling ratio test results. The sequential cross-linked double-network tough hydrogel maintains the temperature responsive property of original PNIPAAm hydrogel. It swells at the low temperature and shrinks at high temperature. The transition temperature is around 30 °C ~ 35 °C. Similarly, the sequential cross-linked tough hydrogel swells further at the low temperature than pure PNIPAAm does.

	Tensile Modulus (kPa)	Strength (kPa)	Strain at break	Toughness (J/m3)
PNIPAAm + Alginate + Ca2+	15.5 ~ 17.1	7.2 ~ 8.1	54 % ~ 58 %	2,390 ~ 2,730
PNIPAAm + Alginate	~ 0.6	~ 0.65	~ 120%	~ 350
Pure PNIPAAm	~ 1	~ 1	~ 100 %	~ 600

Table 4-7 Mechanical properties of different types of sample

4.5 Conclusion

In this chapter, we presented a method to improve the mechanical property of PNIPAAm temperature responsive hydrogel by introducing ionic cross-linked alginate network to covalent cross-linked PNIPAAm network structure.

We fabricated the PNIPAAm-alginate double-network hydrogel by ionically and covalently cross-link the polymer simultaneously and test its mechanical property by the tensile test. We also investigate whether this tough hydrogel maintains the temperature responsive property by doing the swelling ratio test. Based on the experiment results, we found that the mechanical properties of PNIPAAm- alginate double-network hydrogel such as modulus, strength and toughness are improved but the stretchability is decreased. Meanwhile, this tough hydrogel still keeps the temperature responsive property.

Then we sequentially cross-link the PNIPAAm-alginate double-network hydrogel to test whether this mechanical property improvement method also works in a 3D printing process. Therefore, we covalently cross-linked the hydrogel structure first and form the ionic cross-links in the existed structure later.

We obtained the similar experiment results which mean that we can print this temperature responsive double-network hydrogel with improved mechanical property into complex 3D structure.

5. Conclusion and future work

5.1 Conclusion

Poly(N-isopropylacrylamide) (PNIPAAm) is one of the most popular temperature responsive hydrogel which is widely used in various research fields. Projection Micro-StereoLithography (PµSL) is an additive manufacturing method for fabricating 3D complex micro structures. This thesis applies PµSL technique to the PNIPAAm temperature responsive hydrogel. This method can not only realize the complex three-dimensional PNIPAAm microstructures but also help reduce responsive time of PNIPAAm structures by allowing for micro scale manufacturing.

The swelling of the PNIPAAm network at the low temperature is determined by the molar ratio of NIPAAm monomer to cross-linker. The shrinkage of the PNIPAAm network at the high temperature is determined by the concentration of chemical species in the solvent. Therefore, the swelling of the PNIPAAm at the low temperature can be independently controlled by modifying the molar ratio of NIPAAm monomer to cross-linker and keeping the NIPAAm monomer concentration constant; the shrinkage of the PNIPAAm at the high temperature can be independently controlled by changing the concentration of chemical species in the solvent and fixing the molar ratio of NIPAAm monomer to cross-linker constant.

The PNIPAAm hydrogel can be printed by Projection Micro-stereolithography system. During the printing process, both chemicals in photo-curable resin and printing process parameters have effects on the swelling behavior of printed PNIPAAm samples. Swelling at low temperature can be controlled by modifying the molar ratio of NIPAAm monomer to cross-linker. Shrinkage at high temperature can be controlled by modifying the concentration

of chemical species in the solvent or changing the gray scale of projection images. Transition temperature can be shifted to a higher temperature range by introducing MAPTAC ionic monomer in PNIPAAm network. Isotropic swelling behavior change both at the low and the high temperature can be achieved by varying layer thickness of the printing process. The temperature responsive swelling of a chess piece, temperature controlled gripper and sequential deformation dumbbell are presented as demonstration examples of 3D printed PNIPAAm micro structures.

By introducing alginate to the PNIPAAm network, the PNIPAAm-alginate double-network tough hydrogel has the enhanced mechanical properties such as modulus, strength and toughness. However, this method does not have positive effect on stretchability. Meanwhile, temperature responsive property is maintained. Sequential cross-linking method is applied to 3D print temperature responsive PNIPAAm-alginate double-network hydrogel with improved mechanical property.

5.2 Future work

1. The temperature dependent mechanical property of printed PNIPAAm hydrogel has to be studied. The Young's modulus of PNIPAAm hydrogel is not only related to the NIPAAm monomer concentration but also dependent on the temperature. The general trend observed is that the Young's modulus of the PNIPAAm hydrogel increases as the temperature increases. To better understand the PNIPAAm material and to use this temperature responsive hydrogel in more application especially the case where different kinds of motion happen, the information of temperature dependent mechanical property is needed to be found in the future. Because of the micro structure size of printed PNIPAAm sample, it is difficult to use traditional compression test to measure the mechanical property.

2. It is necessary to measure the swelling and the shrinkage force of printed temperature responsive PNIPAAm hydrogel. The PNIPAAm hydrogel swells upon absorbing water at low

temperature and shrinks upon expelling water out of its network at the high temperature. If the deformation is constrained, the swelling or shrinkage generates the force. The information of swelling and shrinkage force is very important in many PNIPAAm hydrogel applications, such as the PNIPAAm temperature responsive valve.

3. Even though we have proved that the sequential cross-linking process can be used to print the PNIPAAm tough hydrogel, further studied are needed in the tough hydrogel study. Firstly, by varying the weight ratio of NIPAAm to alginate, we can improve the mechanical property at different level. In this thesis, I only try 6:1, 8:1 and 10:1 weight ratio and choose tough hydrogel fabricated using 8:1 weight ratio as my standard to compare with pure PNIPAAm. We need the results from different weight ratio cases to find which weight ratio give us the best improved mechanical property.

Secondly, we cannot clearly explain why the PNIPAAm-alginate double-network hydrogel is able to swell further at the low temperature currently. We may need to find out whether there is chemical bond between amine groups on the PNIPAAm chains and carboxyl groups on alginate chains by the FTIR. Furthermore, we need to improve the experimental setup for the tensile test. Currently, we machined the grippers by ourselves and add sand papers on the gripper to increase the friction when they stretch the samples. However, they sometimes suffer from a sliding problem while stretching samples and breaking the samples while loading them. Some new ideas such as using chemical bonds between test sample and the gripper surface may deserve a try. Finally, the main problem for us to print the PNIPAAm-alginate double-network hydrogel in the PµSL system is that the alginate is only solvable in deionized water instead of ethanol. The photo initiator (Phenylbis (2,4,6-tri-methylbenzoyl) phosphine oxide) we currently use for PµSL system is not water solvable. The thermal initiator (Ammonium persulfate) that we use to investigate the double-network ideas is solvable in deionized water but it has very fast cross-linking rate under UV light source. Therefore, in the future, we need to find the alternative photo initiator, which can dissolve in water as alginate does, and has controllable photo-polymerization rate.

References

[1] Ahmed, Enas M. "Hydrogel: Preparation, characterization, and applications: A review." Journal of advanced research 6.2 (2015): 105-121.

[2] Peppas, N. A., et al. "Physicochemical foundations and structural design of hydrogels in medicine and biology." Annual review of biomedical engineering 2.1 (2000): 9-29.

[3] Ono, Toshikazu, et al. "Lipophilic polyelectrolyte gels as super-absorbent polymers for nonpolar organic solvents." Nature materials 6.6 (2007): 429-433.

[4] Yaszemski, Michael J., et al., eds. Tissue engineering and novel delivery systems. CRC Press, 2003.

[5] Slaughter, Brandon V., et al. "Hydrogels in regenerative medicine." Advanced materials 21.32- 33 (2009): 3307-3329.

[6] Li, Yuhui, et al. "Magnetic hydrogels and their potential biomedical applications." Advanced Functional Materials 23.6 (2013): 660-672.

[7] Patel, Alpesh, and Kibret Mequanint. Hydrogel biomaterials. INTECH Open Access Publisher, 2011.

[8] Salem, Aliasger K., et al. "Porous polymer and cell composites that self- assemble in situ." Advanced Materials 15.3 (2003): 210-213.

[9] Gehrke, Stevin H. "Synthesis, equilibrium swelling, kinetics, permeability and applications of environmentally responsive gels." Responsive gels: volume transitions II. Springer Berlin Heidelberg, 1993. 81-144.

[10] Pasparakis, George, Alan Cockayne, and Cameron Alexander. "Control of bacterial aggregation by thermoresponsive glycopolymers." Journal of the American Chemical Society 129.36 (2007): 11014-11015.

[11] Ding, Zhongli, et al. "Size-dependent control of the binding of biotinylated proteins to streptavidin using a polymer shield." Nature 411.6833 (2001): 59-62.

[12] Zou, Yuquan, Donald E. Brooks, and Jayachandran N. Kizhakkedathu. "A novel functional polymer with tunable LCST." Macromolecules 41.14 (2008): 5393-5405.

[13] Jain, Kamiya, et al. "Tunable LCST behavior of poly (N-isopropylacrylamide/ionic liquid) copolymers." Polymer Chemistry 6.38 (2015): 6819-6825.

[14] Okano, Masamichi Nakayama Teruo, and Françoise M. Winnik. "Poly (N isopropylacrylamide)-based Smart Surfaces for Cell Sheet Tissue Engineering." Material Matters 5 (2010): 56.

[15] Wang, Jing, et al. "Self-actuated, thermo-responsive hydrogel valves for lab on a chip." Biomedical Microdevices 7.4 (2005): 313-322.

[16] Wu, Jingjun, Yuteng Lin, and Jianzhong Sun. "Anisotropic volume change of poly (N-isopropylacrylamide)-based hydrogels with an aligned dual-network microstructure." Journal of Materials Chemistry 22.34 (2012): 17449-17451.

[17] Jiang, Shaohua, et al. "Unusual and Superfast Temperature- Triggered Actuators." Advanced Materials 27.33 (2015): 4865-4870.

[18] Stoychev, Georgi, et al. "Hierarchical multi- step folding of polymer bilayers."Advanced Functional Materials 23.18 (2013): 2295-2300.

[19] Dong, Liang, et al. "Adaptive liquid microlenses activated by stimuli-responsive hydrogels." Nature 442.7102 (2006): 551-554.

[20] Serres, Anne, Miroslav Baudyš, and Sung Wan Kim. "Temperature and pH-sensitive polymers for human calcitonin delivery." Pharmaceutical research 13.2 (1996): 196-201.

[21] Luo, Qiaofang, et al. "Lead- sensitive PNIPAM microgels modified with crown ether groups." Journal of Polymer Science Part A: Polymer Chemistry 48.18 (2010): 4120-4127.

[22] Li, Yuhui, et al. "Magnetic hydrogels and their potential biomedical applications." Advanced Functional Materials 23.6 (2013): 660-672.

[23] Schmidt, Stephan, et al. "Adhesion and mechanical properties of PNIPAM microgel films and their potential use as switchable cell culture substrates."Advanced Functional Materials 20.19 (2010): 3235-3243.

[24] Hu, Xiaobo, Zhen Tong, and L. Andrew Lyon. "Control of poly (N-isopropylacrylamide) microgel network structure by precipitation polymerization near the lower critical solution temperature." Langmuir 27.7 (2011): 4142-4148.

[25] Na, Jun- Hee, et al. "Programming reversibly self- folding origami with micropatterned photo- crosslinkable polymer trilayers." Advanced Materials 27.1 (2015): 79-85.

[26] Silverberg, Jesse L., et al. "Origami structures with a critical transition to bistability arising from hidden degrees of freedom." Nature materials 14.4 (2015): 389-393.

[27] Gladman, A. Sydney, et al. "Biomimetic 4D printing." Nature materials (2016).

[28] Shi, Wentao, et al. "3D printing scaffolds with hydrogel materials for biomedical applications." European Journal of BioMedical Research (2015)

[29] http://blogs.wsj.com/corporate-intelligence/2014/04/15/how-a-chinese-company-built-10-homes-in-24-hours/?mod=e2fb

[30] http://www.nanoscribe.de/files/5014/2062/6360/Flyer_PPGT_web.pdf

[31] Zein, Iwan, et al. "Fused deposition modeling of novel scaffold architectures for tissue engineering applications." Biomaterials 23.4 (2002): 1169-1185.

[32] Bandyopadhyay, Amit, et al. "Processing of piezocomposites by fused deposition technique." Journal of the American Ceramic Society 80.6 (1997): 1366-1372.

[33] Tan, K. H., et al. "Scaffold development using selective laser sintering of polyetheretherketone–hydroxyapatite biocomposite blends." Biomaterials24.18 (2003): 3115-3123.

[34] Chung, Haseung, and Suman Das. "Processing and properties of glass bead particulate-filled functionally graded Nylon-11 composites produced by selective laser sintering." Materials Science and Engineering: A 437.2 (2006): 226-234.

[35] Agarwala, Mukesh, et al. "Direct selective laser sintering of metals." Rapid Prototyping Journal 1.1 (1995): 26-36.

[36] Williams, K., et al. "Freeform fabrication of functional microsolenoids, electromagnets and helical springs using high-pressure laser chemical vapor deposition." (1999)

[37] Cohen, Adam, et al. "EFAB: rapid, low-cost desktop micromachining of high aspect ratio true 3-D MEMS.", 1999)

[38] Zhang, Xiang, X. N. Jiang, and C. Sun. "Micro-stereolithography of polymeric and ceramic microstructures." Sensors and Actuators A: Physical 77.2 (1999): 149-156.

[39] Bakarich, Shannon E., Robert Gorkin, and Geoffrey M. Spinks. "4D printing with mechanically robust, thermally actuating hydrogels." Macromolecular rapid communications 36.12 (2015): 1211-1217.

[40] Sun, C., et al. "Projection micro-stereolithography using digital micro-mirror dynamic mask." Sensors and Actuators A: Physical 121.1 (2005): 113-120.

[41] Xia, Chunguang, Howon Lee, and Nicholas Fang. "Solvent-driven polymeric micro beam device." Journal of Micromechanics and Microengineering 20.8 (2010): 085030.Z

[42] Lee, Howon, et al. "Prescribed pattern transformation in swelling gel tubes by elastic instability." Physical review letters 108.21 (2012): 214304.

[43] heng, Xiaoyu, et al. "Ultralight, ultrastiff mechanical metamaterials." Science 344.6190 (2014): 1373-1377.

[44] Ge, Qi, et al. "Multimaterial 4D printing with tailorable shape memory polymers." Scientific Reports 6 (2016).

[45] Yamakawa, Hiromi, and Takenao Yoshizaki. Helical wormlike chains in polymer solutions. Vol. 1. Berlin: Springer, 1997.

[46] Hu, Xiaobo, et al. "Synthesis and dual response of ionic nanocomposite hydrogels with ultrahigh tensibility and transparence." Polymer 50.8 (2009): 1933-1938.

[47] Hernández, Rosa Ma, et al. "Microcapsules and microcarriers for in situ cell delivery." Advanced drug delivery reviews 62.7 (2010): 711-730.

[48] Matzelle, T. R., et al. "Micromechanical properties of "smart" gels: Studies by scanning force and scanning electron microscopy of PNIPAAm." The Journal of Physical Chemistry B 106.11 (2002): 2861-2866.

[49] Maldonado- Codina, Carole, and Nathan Efron. "Impact of manufacturing technology and material composition on the mechanical properties of hydrogel contact lenses." Ophthalmic and Physiological Optics 24.6 (2004): 551-561.

[50] Kobayashi, Masanori, and Masanori Oka. "Composite Device for Attachment of Polyvinyl Alcohol- hydrogel to Underlying Bone." Artificial organs 28.8 (2004): 734-738.

[51] Sun, Jeong-Yun, et al. "Highly stretchable and tough hydrogels." Nature 489.7414 (2012): 133-136.

[52] Lake, G. J. "Fatigue and fracture of elastomers." Rubber Chemistry and Technology 68.3 (1995): 435-460.

[53] Gong, Jian Ping. "Why are double network hydrogels so tough?" Soft Matter 6.12 (2010): 2583-2590.

Appendix A

A.1 Temperature dependent Young's modulus

Mechanical properties of the PNIPAAm films or the single PNIPAAm particles were studied by nanoindenation techniques. The general trend observed is that the young's modulus increases as the temperature is increased. Some measurement of the PNIPAAm hydrogel surface shows that Young's modulus of the PNIPAM hydrogel in swollen state (at 10◦C) is more than 100 times lower than that in collapsed state (at 35◦C) [1]. Other measurements for individual PNIPAAm microparticle and thin hydrogel film shows 10–15-fold increase in the Young's modulus through the volume phase transition temperature, regardless of the cross-linker type and density [2].

A.2 Measurement methods

A number of techniques were invented to characterize the mechanical properties of hydrogel. AFM is a popular method for studying mechanical properties of hydrogel. AFM examines the surface through a tiny mechanical probe. It serves as soft nanoindenters allowing local elasticity measurements of small and inhomogeneous samples like cells, tissues or hydrogels. Hertz model and Oliver-Pharr model are two most common models used to calculate the Young's modulus information from AFM testing data [3].

Some hydrogel induced phenomenon can also be used to study mechanical properties of hydrogel. When an indenter is pressed into a gel which is submerged in a solvent to a fixed depth, the solvent in the gel migrates. The force on the indenter relaxes as Fig. A.1 shows. According to the theory of poroelasticity, the force relaxation curve for indenter is obtained in a simple form, enabling indentation to be used as a method for determining the elastic constants [4]. The thermal bimorph consists of two materials jointed along their longitudinal axis serving as a single mechanical element [5]. As Fig. A.2 shows, a composite beam with two layers made of different materials. With a uniform temperature rise, the length of two sections change unequally. Because the bilayer materials are tightly joined at the interface,

the beam must curve toward the layer made of material with lower coefficients of thermal expansion. The relationship between curvature and elastic modulus can be expressed in bimorph equation
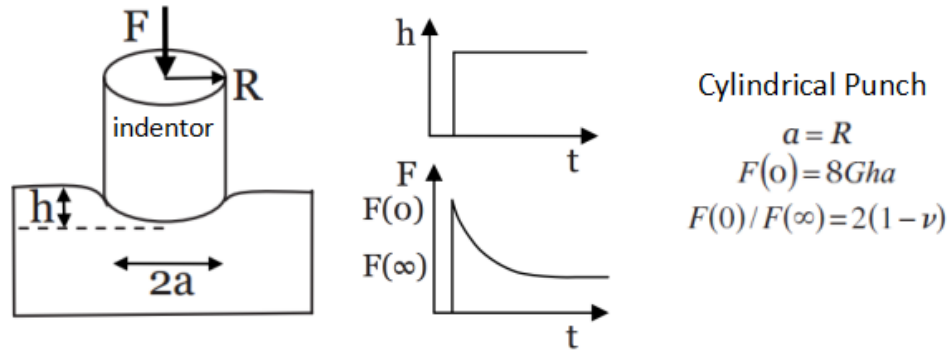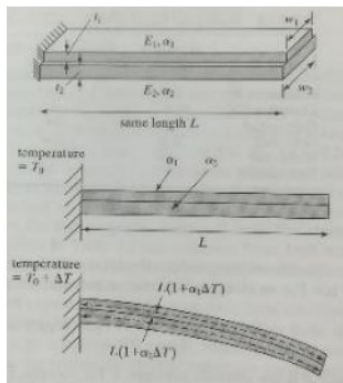

Figure A-1 Force relaxation curve of the indenter that pressed into the gel at a fixed depth (left and middle). The relative equations to find mechanical property of gel (right)

Figure A-2 Thermal bilayer beam bending (left) and formula of bending curvature (right)

A.3 Results and discussion

As the way we prepare samples in temperature responsive property study in Chapter 2, fully cured samples are used for experiments to find the maximum Young's modulus the corresponding NIPAAm resin can reach. Here we use photo-curable resin with 6.2 M NIPAAm monomer and 324 mM cross-linker (without PA) to fabricate all the test samples. PNIPAAm film is 1 mm thick. To make sure the thicker film is fully cured, 6000 mJ cm^{-2} light energy dosage will be used during the UV oven fabrication.

Several methods used for Young's modulus measurement have been tried. Though none of the following methods give us the ideal results, they still help us understand the temperature dependent property and the rough value range of the Young's modulus.

In a word, we still need to find a best way to get modulus information.

A.3.1 Compression test

The compression test is the basic method to get Young's modulus by calculating the slope of stress-strain curve.

Samples are punched out of the PNIPAAm thin film and stored in DI water for over hours. Self-assembled compression test system is used for testing the PNIPAAm samples. A water bath can load the sample inside the chamber and change a sample's temperature with the help of refrigerated circulator. Actual temperature inside the sample chamber can be measured by thermocouple. A motorized stage provides a well-controlled compression process and record the displacement during the process. A load cell which mounted on the moving part of motorized stage records the force during the compression process.
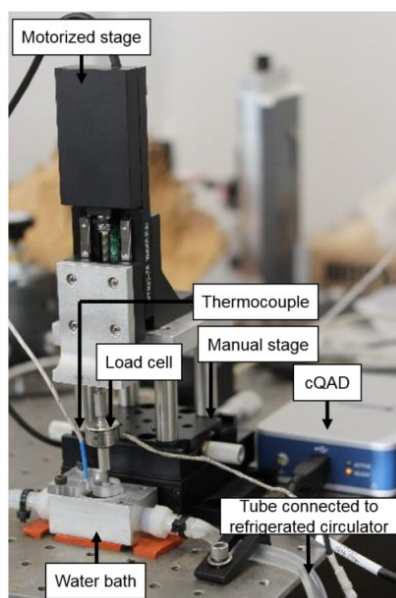

Figure A-3 Custom-built compression test system

Before the compression test, sample is loaded in sample chamber of water bath for a long enough time to get its equilibrium size. After the compression process is finished, the stress-strain curve will automatically generate based on displacement and force data.
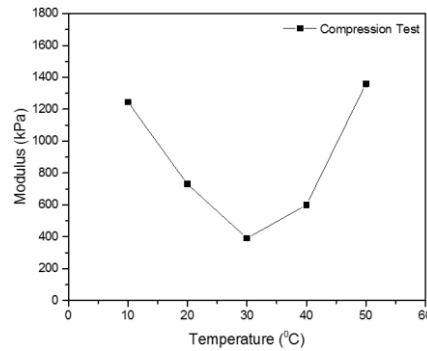
Figure A-4 Compression test results

Figure A.4 shows the Young's modulus at different temperature. The modulus is around 1300 kPa at 10 °C. As temperature increases, modulus decreases to lowest level, around 400 kPa, at around transition temperature (around 30 °C) and then increase to around 1400 kPa at 50 °C. The value and tendency of modulus in the low temperature range are different from our expectation.

The reason may be that in the low temperature range, the PNIPAAm sample swells and contains lots of water inside. The compression process is a relative fast process to let water stored in the PNIPAAm sample move out compared to the free movement of water molecular. Therefore, the measured compressive force actually also includes the force that squeezes water out of the structure. This accounts for the higher modulus value. As temperature increase, the water molecular moves faster as it becomes more and more active. The force needed to squeeze water out is smaller. Therefore, the measured modulus is getting smaller as temperature increases. In the high temperature range, the PNIPAAm sample shrinks and contains less water inside. The measured modulus tends to be the property of PNIPAAm itself.

A.3.2 Rheometer test

Rheometer test is typical method for finding viscoelastic property of hydrogel.

Samples are punched out of the PNIPAAm thin film and stored in DI water for additional hours. Rheometer (*Malvern Kinexus series*) is used for measurement. Because of the swelling behavior of the sample, the parameter (cross-section area) of the rotation plate needs to be

modified at different temperature to get precise modulus value. The storage modulus is measured and then transferred to Young's modulus. Modulus of PNIPAAm hydrogel is rate dependent and we use low rate test range to get modulus in rubbery state in which modulus is at low value plateau.
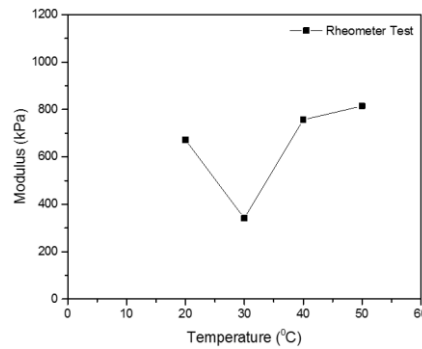

Figure A-5 Rheometer test results.

Figure A.5 shows the Young's modulus (transferred from storage modulus) at different temperature. Modulus is around 700 kPa at 20 °C. As temperature increases, modulus decreases to lowest level, around 300 kPa, at around transition temperature (30 °C) and then increase to around 900 kPa at 50 °C. The values and tendency of modulus are same as those we get from compression test which different from our expectation.

The same reason may explain this phenomenon. When shear force is added on the PNIPAAm samples in low temperature range, large amount of water contained inside the PNIPAAm may has some influence on the measurement.

A.3.3 Force relaxation test

Force relaxation property is the unique property of hydrogel and force relaxation curve can help to find modulus based on the equation in Fig. A.1.

Samples are the PNIPAAm thin films and stored in DI water for over hours. Self-assembled compression test system can also be used. We compress the sample 5 % of its height and give it long enough time for force relaxation. We collect the compressive force of the PNIPAAm samples data over hours and use this equation and get the Young's modulus value.
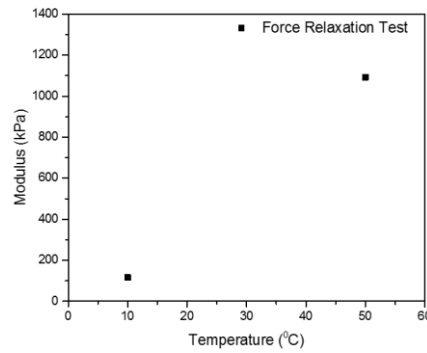
Figure A-6 Force relaxation test results

Figure A.6 shows the Young's modulus at two temperatures. Modulus is around 100 kPa at 10 °C. As temperature increases, modulus then increase to around 1100 kPa at 50 °C. The value and tendency of modulus seems very good but actually the sample for the test is not qualified since the size difference between indenter and sample is not big enough to satisfy the theory of equation. This will not give precise modulus information.

A.3.4 Bimorph bending test

Bilayer structure will bend to certain configuration of curvature when thermal expansion mismatch between two materials happens. We can get Young's modulus value using bimorph equation.
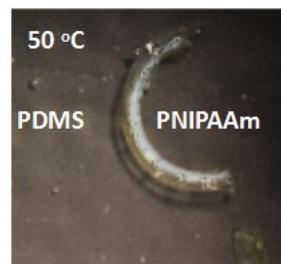

Figure A-7 Bimorph bending phenomenon

We use PDMS as the second material to get information about the PNIPAAm mechanical property. PDMS is well-known material whose mechanical property is easily measured. We fabricate PDMS thin film first and treat the surface with benthophene (*Sigma-Aldrich*) to strengthen the bond between PDMS and PNIPAAm. Then PNIPAAm is directly polymerized on the top of treated PDMS using sandwich structure. Finally, we cut the bilayer film into

desirable size for measurement. The film will be put into a temperature-controllable chamber filled with DI water. The image of bilayer film with different curvature configuration is taken at different temperature. Therefore, the curvature can be measured. We know the dimension of two films and the mechanical property of PDMS. Using the equation, we can find the modulus of PNIPAAm.
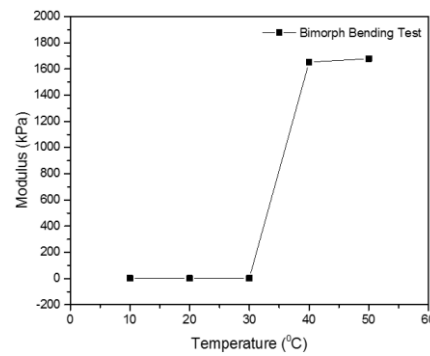

Figure A-8 Bimorph bending test results

Figure A.8 shows the Young's modulus at different temperature. Modulus is smaller than 1 kPa at 10 $^{\circ}$C. As temperature increases, keep increasing and reach to 1700 kPa at 50 $^{\circ}$C. The tendency of modulus is same as our expectation but the value in low temperature range is unreasonable small.

This method does not use any external force which prevents the influence of water inside the PNIPAAm. However, the bond between PDMS and PNIPAAm is not so perfect that may explain why the value of modulus is too small in low temperature range.

A.3.5 AFM

The atomic force microscope (AFM) is the most popular method for studying mechanical properties of hydrogel.

We prepare PNIPAAm thin film and stored in DI water for additional hours. There are some problems when we measure the samples. Firstly, we cannot realize temperature control. To control the temperature by changing ambient atmosphere is not precise and using the temperature accessory is too expansive. Secondly, the PNIPAAm should be immersed in water and measured. This causes a lot of hard time for us to find the surface of the sample.

Reference A

[1] Wang, Jilong, et al. "Ion-linked double-network hydrogel with high toughness and stiffness." Journal of Materials Science 50.16 (2015): 5458-5465.

[2] Burmistrova, Anna, et al. "Effect of cross-linker density of P (NIPAM-co-AAc) microgels at solid surfaces on the swelling/shrinking behaviour and the Young's modulus." Colloid and Polymer Science 289.5-6 (2011): 613-624.

[3] Liu, Tong. "Developing Applications of Atomic Force Microscopy in Cellular Imaging and Mechanical Property Measurement." (2014).

[4] Hu, Yuhang, et al. "Using indentation to characterize the poroelasticity of gels." Applied Physics Letters 96.12 (2010): 121904.

[5] Liu, Chang. Foundations of MEMS. Pearson Education India, 2012.